

# CHEM MED CHEM

CHEMISTRY ENABLING DRUG DISCOVERY

## Accepted Article

**Title:** Experimental and computational evaluation of some piperonylic acid derived hydrazones bearing isatin moiety as dual inhibitors of cholinesterases and monoamine oxidases

**Authors:** Senthil Raja Ayyannan, Vishnu M S, Pavankumar V, and Sandeep Kumar

This manuscript has been accepted after peer review and appears as an Accepted Article online prior to editing, proofing, and formal publication of the final Version of Record (VoR). This work is currently citable by using the Digital Object Identifier (DOI) given below. The VoR will be published online in Early View as soon as possible and may be different to this Accepted Article as a result of editing. Readers should obtain the VoR from the journal website shown below when it is published to ensure accuracy of information. The authors are responsible for the content of this Accepted Article.

**To be cited as:** *ChemMedChem* 10.1002/cmdc.201900277

**Link to VoR:** <http://dx.doi.org/10.1002/cmdc.201900277>

WILEY-VCH

[www.chemmedchem.org](http://www.chemmedchem.org)

A Journal of



# Experimental and computational evaluation of some piperonylic acid derived hydrazones bearing isatin moiety as dual inhibitors of cholinesterases and monoamine oxidases

Vishnu M S, Pavankumar V, Sandeep Kumar, Senthil Raja A<sup>\*[a]</sup>

[a] Vishnu M S, Pavankumar V, Senthil Raja A

Pharmaceutical Chemistry Research Laboratory, Department of Pharmaceutical Engineering & Technology,  
Indian Institute of Technology (Banaras Hindu University)  
Varanasi 221005, Uttar Pradesh (India) Fax: (+91)542-2368428  
E-mail: asraja.phe@iitbhu.ac.in

## Abstract

A set of piperonylic acid derived hydrazones with variable isatin moiety was synthesized and evaluated for their inhibitory activity against the enzymes acetylcholinesterase (AChE), butyrylcholinesterase (BChE), and monoamine oxidase A and B (MAO-A/B). The results of the *in vitro* studies revealed compounds possessing IC<sub>50</sub> values in the micromolar range, with the majority of them showing higher selectivity towards MAO-B isoform. The compound N-(2-oxo-1-(prop-2-ynyl)indolin-3-ylidene)benzo[d][1,3]dioxole-5-carbohydrazide (compound **3**) was identified as lead AChE inhibitor with IC<sub>50</sub> = 0.052 ± 0.006 μM while N-[(3E)-5-chloro-2-oxo-2,3-dihydro-1H-indol-3-ylidene]-2H-1,3-benzodioxole-5-carbohydrazide (compound **2**) proved to be a lead MAO-B inhibitor with IC<sub>50</sub> = 0.034 ± 0.007 μM, possessing 50 times more selectivity than MAO-A. The kinetic studies revealed that compounds **2** and **3** displayed competitive and reversible inhibition of AChE and MAO-B respectively. The molecular docking studies revealed the significance of hydrophobic interactions along the active site pocket of the enzymes under inspection. Further lead optimization studies can favor the development of potential neurotherapeutic agents.

## Introduction

Monoamine oxidases (MAOs) are an important family of enzymes which have been extensively explored in the treatment of depression among patients worldwide. The MAO enzymes comprise 2 isozymes: MAO-A and MAO-B. The former has a high affinity towards substrates serotonin and norepinephrine, while the latter prefers phenyl ethylamine and benzylamine. These enzymes are

homologous and share 70% similarity with respect to structure, both containing the cofactor flavin adenine dinucleotide (FAD) covalently bonded to the amino acid cysteine (Cys406 and Cys397 for MAO-A and MAO-B respectively)<sup>[1]</sup>. MAO-B enzyme is distributed in the CNS, while the MAO-A isozyme is more profound in the peripheral parts of the body. These enzymes metabolize the substrates via the oxidative deamination process, resulting in the generation of hydrogen peroxide (H<sub>2</sub>O<sub>2</sub>), ammonia (NH<sub>3</sub>) and the aldehyde metabolite of the substrate. The generated H<sub>2</sub>O<sub>2</sub> diffuses into neighboring cells and takes part in the generation of reactive oxygen species (ROS) which results in apoptosis and cell death<sup>[2]</sup>.

The cholinesterase (ChE) family, consisting of acetylcholinesterase (AChE) and butyrylcholinesterase (BChE), are important enzymes, mainly localized between the synaptic cleft and glial cells<sup>[3]</sup>. It serves the function of hydrolyzing the acetylcholine (ACh) and butyrylcholine (BCh) neurotransmitter respectively, resulting in the termination of cholinergic neurotransmission from the brain to the peripheral parts of the body. ACh plays a pivotal role in the management of learning and memory processing.

Both the MAOs and ChEs are important biomarkers in the diagnosis of advanced stages of Alzheimer's disease (AD) and Parkinson's disease (PD). The MAO-B levels are shown to be elevated to 3~4 folds on aging neurons, while MAO-A concentration is estimated to be ~6 folds greater in cardiovascular tissues<sup>[4]</sup>. MAO mediated ROS generation results in many pathological conditions including cardiovascular diseases (MAO-A) and neurodegeneration (MAO-B), some of the leading causes of death in the present world. The oxidative stress induced disintegration of neurons is an important model which has guided in the development of some of the important marketed MAO-B inhibitors, which include selegiline, rasagiline, and safinamide, to treat AD and PD. The availability of a wealth of co-crystallized structures, more than 40 in number, for the MAO-B isozyme has tremendously favored research in the development and validation of virtual lead compounds via the application of high throughput virtual screening and molecular modeling methodologies. It has been revealed that in patients with AD, the serum levels of AChE and BChE are elevated to a great extent, leading to an uncontrolled reduction in the levels of ACh, which causes an imbalance in motor coordination and, problems in cognition and memory. It has been identified that the BChE activity is increased 40-90% than the normal conditions in the critical parts of the brain in AD diagnosed patients, while the AChE activity is shown to be either reduced or steady<sup>[5]</sup>. This intensifies the symptoms associated with AD and therefore proves to be a good target to develop potential inhibitors to bring equilibrium to the induced drastic conditions. At present, four AChE inhibitor drugs are approved to

treat the symptomatic effects of AD, namely tacrine, galantamine, donepezil, and rivastigmine. Lately, the enzyme BChE has shown great promise in the development of non-selective AChE/BChE inhibitors in AD symptomatic treatment as well<sup>[6,7]</sup>. The contemporary research has shown an exponential increase in the drug candidates developed as inhibitors of ChE in the clinical pipeline, but a significant amount fails due to adverse side effects towards the conclusion of one phase study. As of now the suggested approach to treat AD with the available drugs is to incorporate individualization and adjustment in the current treatment regime according to the age and gender.

According to the National Institute of Aging (2016 report), National Institute of Health (NIH), AD is among the six leading causes of death in the USA<sup>[8]</sup>. It is estimated that approximately 5.7 million people are suffering from AD in the USA alone. Reports from WHO show an estimate of 47.5 million people worldwide living with dementia. The total number of individuals with Alzheimer's dementia is anticipated to rise number to 75.6 million peoples in 2030 and 135.5 million peoples in 2050, with the majority of sufferers living in low and middle-income countries (Alzheimer's, 2014)<sup>[9]</sup>. Out of all the major treatment difficulties the “effectiveness of current treatment regimens” poses a major issue of concern. And for this reason, modification of the disease pathway by means of neuroprotective therapy is an essential unmet clinical necessity. During the period 2000 to 2015, a staggering 123% increase in mortality was observed in patients with AD. About 112 drug candidates are being tested in the clinical pipeline as of 2018, out of which 26 candidates are in Phase III trials<sup>[10]</sup>. Though the number of clinical candidates is soaring high, there is also a substantial decline in the progress to the next level of evaluation, owing to the rise in toxicity concerns and efficacy issues.

In 2014, the first multi-therapy formulation, Namzaric®, was developed, which is a combination of NMDA receptor antagonist, memantine, and AChE inhibitor donepezil hydrochloride<sup>[11]</sup>. This regimen has brought about a major shift in the current treatment methodology with an added benefit of targeting multiple pathways to AD pathogenesis. Ladostigil, a dual inhibitor of ChE and MAO has recently been developed and has now entered the Phase IIb clinical pipeline. The molecule is composed of a carbamate skeleton and a propargylamine chain, resembling rasagiline structure<sup>[12]</sup>. It is a selective inhibitor of the MAO-B enzyme and ChE and has shown to lower 1-methyl-4-phenyl-1,2,3,6-tetrahydropyridine (MPTP) toxicity in PD animal models<sup>[13]</sup>. The success of this molecule in the phase I trials has given an insight into targeting the ChE and MAO pathways to AD and PD.

Science as of today has diversified approaches to treating these diseases and one of the most interesting approaches being the development of chemical entities to target the particular enzymes responsible for

the disease condition. From single targeting to dual targeting, the approach has gained a lot of insight into the world of neurotherapeutics. When the single targeting failed to improve upon the disease state, a new methodology was adapted so as to tackle this rising problem, which surfaced much earlier than expected as the now prominent multi target-directed ligands (MTDLs) to treat diseases with multifaceted pathophysiology as in the case of AD and PD<sup>[14]</sup>. This not only poses a challenge but a great venture to discover new agents and possible druggable targets. To treat such diseases the viable macromolecules, which include mainly the enzymes and receptors, are studied in depth to identify regions of selectivity, activity, and other allosteric sites, in case of explored targets, giving the effect necessary for possible treatment. All in all, there are more than fifty known target enzymes for neurodegeneration available till date, having pivotal roles in the disease conditions mentioned above. The study of these protein targets in great detail has been made possible through the development of Protein Data Bank (PDB), which provides a library of bound and unbound crystal structures of the enzymes in all of their known conformations<sup>[15]</sup>. Such tools have greatly enhanced the conception of novel ideas in the development of new molecules with the required features to adapt and target the enzyme at the right spatial orientation so as to facilitate the much anticipated neuroprotective action.

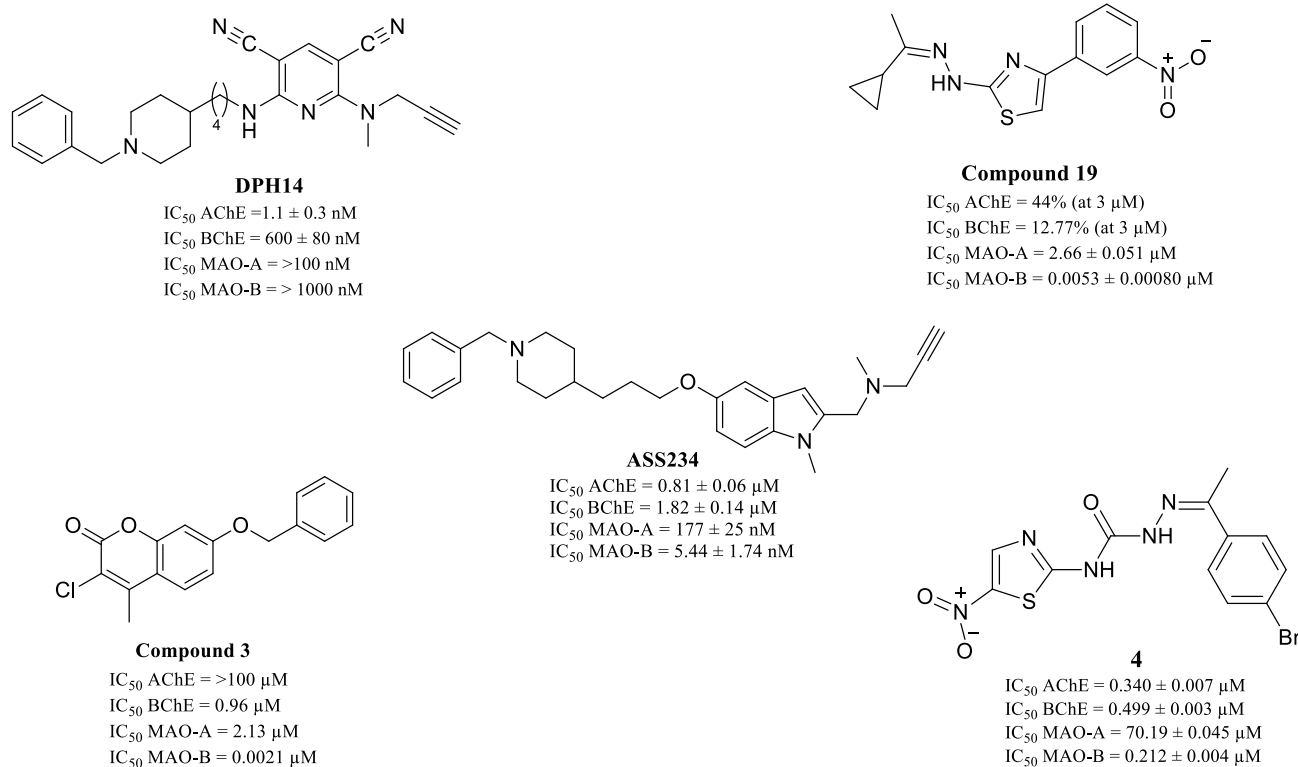


**Figure 1.** Some developed MTDLs targeting MAO and ChE.

Heterocyclic rings are explored extensively in the synthesis of potent compounds with dual inhibitory properties in the field of neurotherapeutics. Many different naturally occurring scaffolds like coumarins, pyridines, thiazoles, etc. have utilized in the past few years in developing highly potent dual inhibitors of MAO and ChE with IC<sub>50</sub> values within the nanomolar range as shown in **Fig 1**<sup>[16,17,18,19,20]</sup>. Isatin is one of the most important scaffolds with a multifaceted pharmacological profile in the treatment of CNS diseases, especially neurodegenerative disorders like AD, and PD<sup>[21]</sup>. The scaffold has higher selectivity towards MAO-B than MAO-A<sup>[22,23]</sup>, and its oral administration has shown to increase the level of ACh and DA in the rat striatum<sup>[24]</sup>. Owing to its well-tolerated profile in human beings, we propose to explore this versatile scaffold into developing lead molecules as multi-target-directed ligands with dual MAO and ChE<sup>[25]</sup> inhibition properties.

In the previous work, we have identified potential dual inhibitors of MAO-B and AChE possessing a 3,4-methylenedioxy aniline scaffold and a variable aryl moiety connected by a semicarbazino linker of the type: R-NH-(C=O)-NH-N=C-R<sup>1</sup>(R<sup>2</sup>)<sup>[25]</sup>. The present work attempts to replace the semicarbazino bridge with a hydrazone linker, by the removal of NH group present at the amido terminal of the semicarbazino spacer, to further optimize the identified leads. The design approach follows the same strategy as our previous work, by adopting an electron-rich spacer molecule with a greater affinity towards forming hydrogen bonds, in this case, a hydrazone bridge, and attaching hydrophobic aryl groups at the carbimino and amido terminal of the spacer<sup>[26]</sup>. The carbimino terminal was introduced with isatin moiety with varying degree of hydrophobicity and steric properties offered by substituents at N-1 and 5-position. Thus, a series of 10 compounds have been synthesized in the wet-lab, which was further taken up for biological and computational studies. All the test compounds were characterized by FT-IR, <sup>1</sup>H, <sup>13</sup>C, and mass spectrometry methods. The *in vitro* biological evaluation was performed using the AChE, BChE, and MAO-A/B enzyme inhibition assay. Computational docking methodology was explored to correlate and study in depth the binding characteristics of the designed ligand with the target proteins<sup>[27]</sup>. The molecular modeling studies were performed using cheminformatic tools like ChemDraw 12.0 Pro, AutoDock 4.2, Discovery Studios 2017, and Pymol<sup>[28]</sup>. Computational prediction of Drug-likeness and Pharmacokinetic properties were carried out using online platforms such as PKCSM, and Protox servers<sup>[29,30]</sup>.

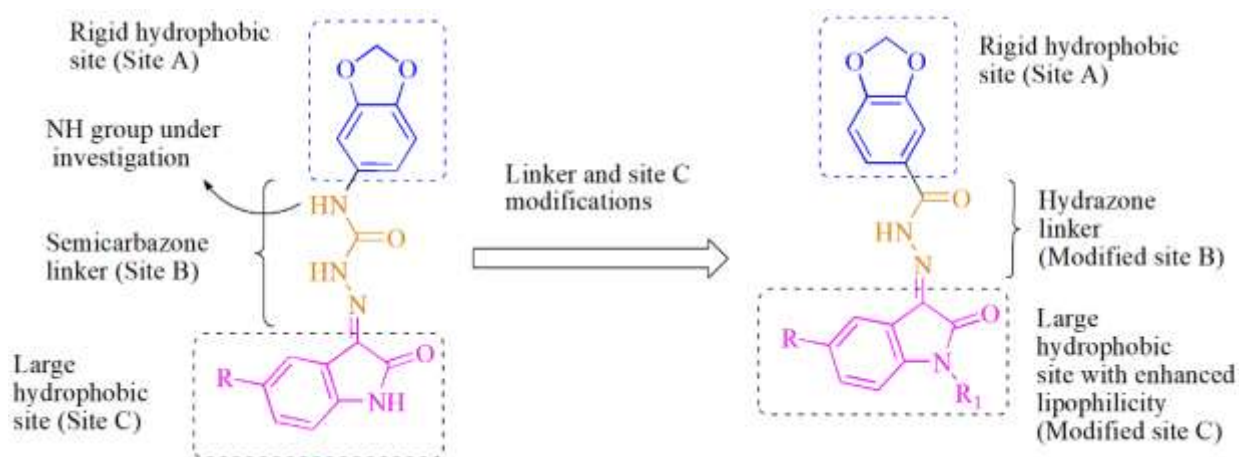
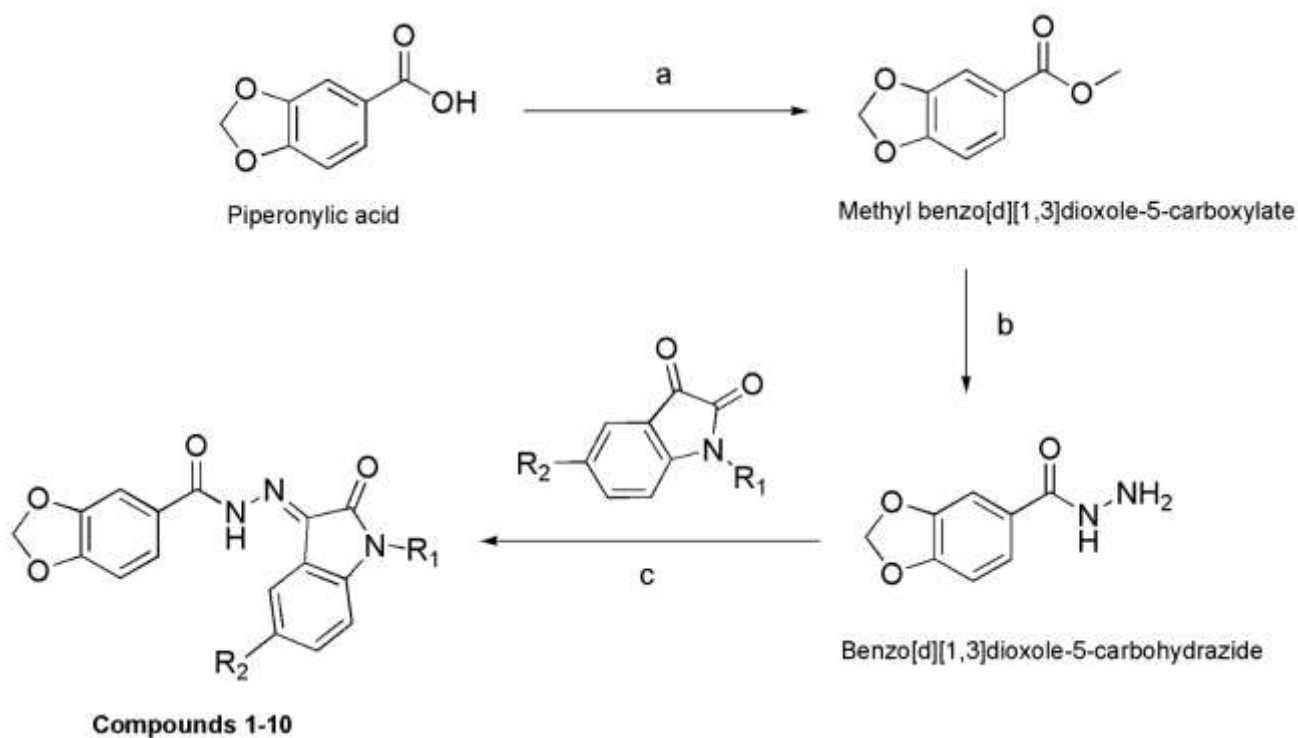


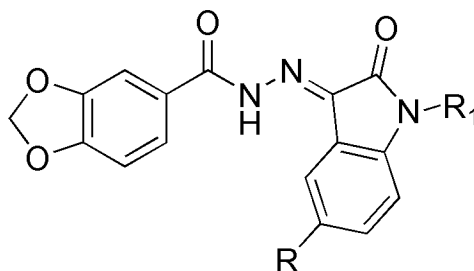
**Figure 2.** The design strategy for piperonylic acid-based hydrazones.

## Results and Discussions



**Scheme 1.** Synthesis of compounds **1-10**. Reagents and conditions: a) conc.  $\text{H}_2\text{SO}_4/\text{MeOH}$ , Reflux,  $80^\circ\text{C}$ , 2 hrs; b)  $\text{EtOH}$ ,  $\text{NH}_2\text{NH}_2 \cdot \text{H}_2\text{O}$ , reflux,  $80^\circ\text{C}$ , 2 hrs; c) glacial  $\text{AcOH}/\text{EtOH}$ , reflux,  $80^\circ\text{C}$ , 2-8 hrs.

## Chemistry

**Table 1.** Physicochemical data for compounds **1-10**.

Compd	R	R <sub>1</sub>	cLogP <sup>[a]</sup>	Yield%	MP [°C]	R <sub>f</sub> <sup>[b]</sup>
<b>1</b>	H	H	2.186	94	266-269	0.64
<b>2</b>	Cl	H	2.899	90.5	286-290	0.72
<b>3</b>	H	C <sub>3</sub> H <sub>3</sub>	3.162	86.5	190-195	0.53
<b>4</b>	H	C <sub>3</sub> H <sub>5</sub>	3.836	84.36	192-194	0.56
<b>5</b>	NO <sub>2</sub>	H	1.929	88.2	295-299	0.78
<b>6</b>	Br	H	3.049	94.6	294-296	0.69
<b>7</b>	H	C <sub>6</sub> H <sub>5</sub> CH <sub>2</sub>	4.83	79.1	210-213	0.44
<b>8</b>	H	4-F-C <sub>6</sub> H <sub>5</sub> CH <sub>2</sub>	4.973	81.5	199-201	0.52
<b>9</b>	Cl	4-F-C <sub>6</sub> H <sub>5</sub> CH <sub>2</sub>	6.256	92.81	196-199	0.40
<b>10</b>	H	2,4-Cl <sub>2</sub> -C <sub>6</sub> H <sub>5</sub> CH <sub>2</sub>	5.686	87.34	220-222	0.42

<sup>[a]</sup> Computational logP value calculated from ChemDraw Pro 12.0.

<sup>[b]</sup> Solvent system: Ethylacetate/n-Hexane 3:7.

The synthesis of piperonylic acid derived hydrazones containing substituted isatin moiety is described in **Scheme 1** from 2H-1,3-benzodioxole-5-carbohydrazide<sup>[31]</sup>. The reaction of piperonylic acid with methanol in the presence of concentrated sulphuric acid produced the ester intermediate methyl 2H-1,3-benzodioxole-5-carboxylate; the hydrazide was prepared by the reaction of the ester with hydrazine monohydrate using ethanol as a solvent by refluxing. Final products **1-10** were prepared in good yields (79 – 94%) by acid-catalyzed condensation of the hydrazone with the appropriate N-substituted and 5-substituted isatin fragments. The physicochemical and spectral data of the final compounds are in great alignment with the structural composition. The physicochemical

characterization data of the final compounds **1-10** are given in **Table 1** and the spectral data are described in the experimental section.

### ***In vitro* ChE inhibition assay**

The *in vitro* inhibition potential of compounds **1-10** against electric eel AChE (eeAChE) was determined using a UV-based spectrophotometric method of Ellman et al., with Donepezil as the reference standard<sup>[25]</sup>. The results of AChE and BChE inhibition assays are expressed in terms of IC<sub>50</sub> values and are summarized in **Table 2**. Absorbance readings were taken in triplicate measure for all the compounds used for the study. The synthesized compounds displayed good activity profile in the AChE inhibition assay, where the IC<sub>50</sub> values are obtained in the micromolar range. Compound **2** displayed the highest activity among the series with an IC<sub>50</sub> value of 0.052 ± 0.006 μM close to the standard drug Donepezil. The second best inhibition profile was observed in the case of compound **3**, which displayed an IC<sub>50</sub> of 0.85 ± 0.107 μM, followed by compound **10**, with an IC<sub>50</sub> of 0.928 ± 0.024 μM. Compound **5** was identified with the lowest activity, an IC<sub>50</sub> of 25.13 ± 2.687 μM.

In the BChE inhibition assay<sup>[20]</sup>, most of the compounds displayed moderate to excellent results as compared to the reference standard Donepezil. Compound **3** was identified with the highest activity among the series, with an IC<sub>50</sub> value of 0.88 ± 0.007 μM, almost comparable to Donepezil standard. Compounds **2** and **8** followed as the next best inhibitors possessing IC<sub>50</sub> values of 0.96 ± 0.005 μM and 0.89 ± 0.085 μM respectively. Similar to AChE inhibition assay results, compound **5** was identified with the lowest IC<sub>50</sub> value among the series, about 13.786 ± 2.163 μM.

Among the series, compounds **8**, **9** and **10** have halogen substituents (chloro and fluoro groups) within the variable aryl region present in the carbimino terminal of the hydrazone spacer. Detailed structure-activity relationship (SAR) studies have been documented for the series after a thorough analysis of the inhibitory activity data from **Table 2**.

**Table 2.** *In vitro* and computational results of ChE inhibition studies for compounds **1-10**.

Compd	AChE			BChE		
	IC <sub>50</sub> [μM] <sup>[a]</sup>	ΔG [kcal mol <sup>-1</sup> ] <sup>[b]</sup>	Ki [μM] <sup>[b]</sup>	IC <sub>50</sub> [μM] <sup>[a]</sup>	ΔG [kcal mol <sup>-1</sup> ] <sup>[b]</sup>	Ki [μM] <sup>[b]</sup>
<b>1</b>	4.72±0.063	-9.91	0.055	1.28±0.067	-8.08	1.19

<b>2</b>	0.052±0.006	-9.73	0.073	0.96±0.005	-9.14	0.199
<b>3</b>	0.85±0.107	-10.47	0.022	0.88±0.007	-8.92	0.288
<b>4</b>	1.925±0.086	-10.37	0.026	5.26±0.753	-8.36	0.746
<b>5</b>	25.13±2.687	-9.31	0.151	13.786±2.163	-8.36	0.744
<b>6</b>	6.95±0.451	-9.91	0.058	8.23±0.068	-9.14	0.198
<b>7</b>	1.272±0.179	-11.55	0.0034	4.48±0.26	-9.84	0.061
<b>8</b>	2.93±0.84	-11.47	0.0039	0.89±0.085	-9.87	0.058
<b>9</b>	5.89±0.223	-11.57	0.0032	1.59±0.58	-9.14	0.2
<b>10</b>	0.928±0.024	-11.51	0.0036	1.64±0.076	-10.06	0.042
<b>DNP</b>	0.021±0.005	-	-	0.78±0.025	-	-

[a] Each IC<sub>50</sub> value is the mean ± SEM. Level of statistical significance: p<.05 versus the corresponding IC<sub>50</sub> values obtained against ChEs, as determined by ANOVA/Dunnett's. Reference inhibitors: DNP – Donepezil.

[b] Computationally predicted values.

### SAR for AChE inhibition

In general, substitution at N-1 position in the isatin ring by bulky aromatic rings and aliphatic side-chains resulted in an overall improvement in the AChE inhibitory activity, as in the case of compounds **3**, **4**, **7**, **8**, and **10**, in comparison with the compound **1**, containing no substitution in the isatin ring. An exception being compound **9**, with para-fluoro benzyl substitution at the R<sub>1</sub> position and chloro substitution at the R<sub>2</sub> position, where the activity was lowered as compared to the unsubstituted derivative, compound **1**. An increase in activity was observed when the R<sub>1</sub> position was substituted by aliphatic propargyl and allyl side chains (compounds **3** and **4**), where the former showed better profile, as compared to compounds substituted by halogenated benzyl derivatives. Substitution at the R<sub>1</sub> position by un/substituted benzyl groups led to an increase in activity. Mono- and Di- substitution at the para and ortho positions of the benzyl groups in the R<sub>1</sub> region gave rise to better AChE activity, as in the case of compounds **8** and **10**, where it was observed that the di-substitution with 2-chloro groups gave a better profile. Substitution at the R<sub>1</sub> position by para-substituted benzyl ring with a fluorine group gave rise to a decrease in AChE inhibitory activity as compared to the other benzyl substituted derivatives. It was observed that the substitutions at the 2<sup>l</sup> and 4<sup>l</sup> positions of the benzyl ring (compound **10**) favor a better activity than the mono-substituted and un-substituted benzyl derivatives, compounds **7**, **8** and **9**. Introduction of the highly electronegative nitro group at the R<sub>2</sub> position of the

isatin moiety, compound **5**, gave rise to a drastic decrease in the AChE inhibitory activity as compared to bromo and chloro substituted derivatives, compounds **6** and **2** respectively. Substitution by bromo group (compound **6**) at the R<sub>2</sub> position gave rise to a decrease in potency as compared to chloro group (compound **2**), which led to a drastic increase in the inhibitory activity, and the un-substituted isatin derivative compound **1**. Substitution at the R<sub>2</sub> and R<sub>1</sub> position by chloro group and p-fluoro benzyl group, respectively, led to a decrease in the inhibitory activity as compared to compounds **1-4**, **7**, **8**, and **10**. Chlorine substitution at the R<sub>2</sub> position, compound **2**, gave the highest activity as compared to the rest of the series.

### SAR for BChE inhibition

The R<sub>1</sub> position of the isatin moiety, when substituted with benzyl groups containing halogen atoms, led to a decrease in the activity as compared to compound **1**, except in the case of compound **8**, where it is substituted with a p-fluoro benzyl group. Disubstitution at 2 and 4 positions by chloro group and mono substitution at the para position by fluoro group in the benzyl ring led to better BChE activity than the un-substituted derivative, as shown by compounds **8**, **9**, and **10** compared to compound **7**. Compound **8** surfaced out with better activity as compared to the benzyl substituted derivatives. Substitution by aliphatic propargyl and allyl group at the R<sub>1</sub> position gave rise to mixed results. In the case of the former, compound **3**, the BChE inhibitory activity was found to be greater than that of the latter, compound **4**. Compound **3** possessed greater inhibitory activity than all the compounds of the series. The R<sub>2</sub> position of the isatin moiety when substituted with bromo group, compound **6**, led to a decrease in activity as compared to the chloro substituted derivative, compound **2**, but showing better activity as compared to compound **5**. Substitution at R<sub>2</sub> position by chloro group and R<sub>1</sub> position by para-substituted fluoro benzyl group, compound **9**, led to a decrease in activity as compared to compound **2** and compound **8**, which are monosubstituted each in the positions described above.

### Kinetic studies of lead AChE inhibitors

To understand the inhibition mechanism of the lead compounds **2** and **3** on AChE, kinetic studies were carried out using eeAChE. The Lineweaver–Burk plots for compound **2** and compound **3** (**Fig 3A** and **Fig 3B**) were linear and intersected at the Y-axis. This pattern shows that both the lead compounds inhibited AChE competitively, and further extrapolation of the results proved that they bind reversibly to AChE.

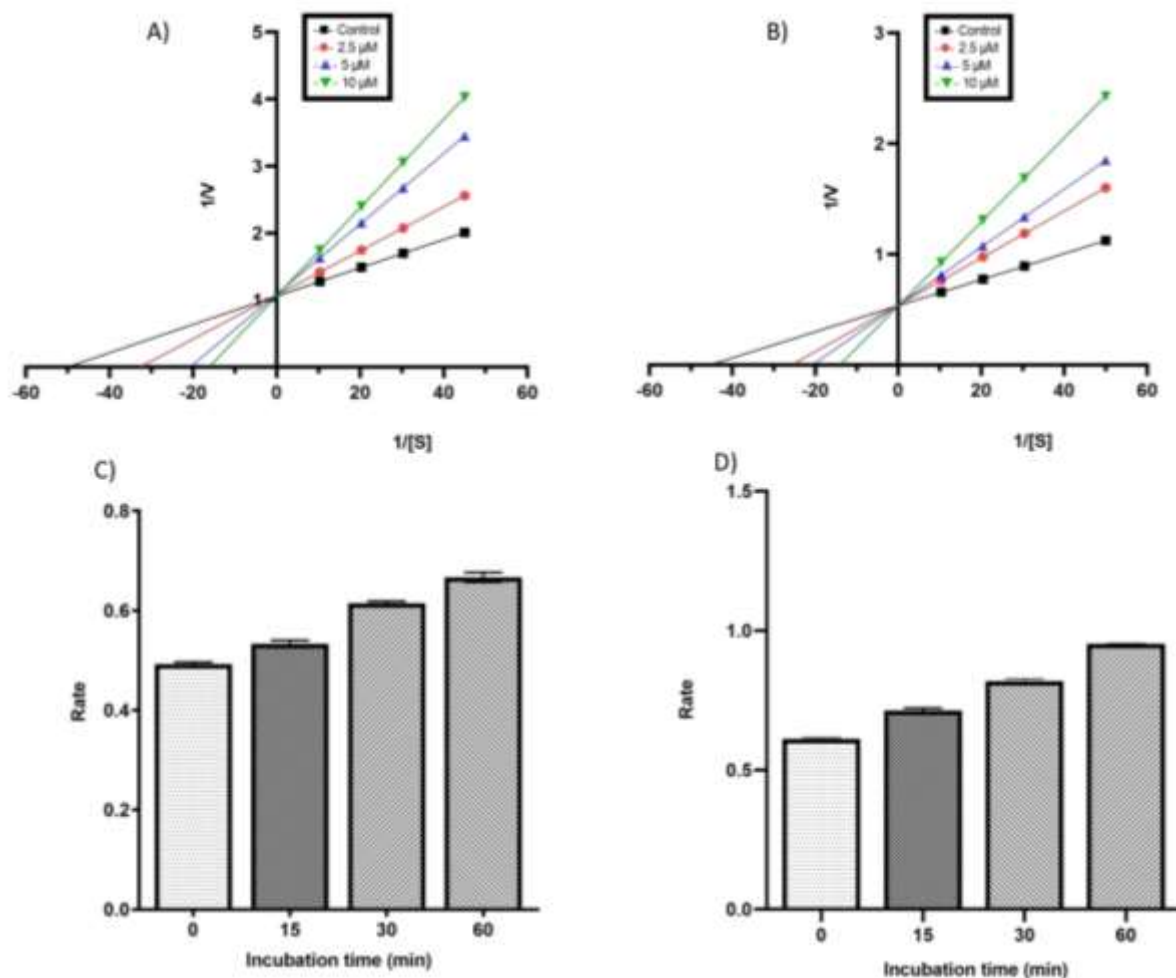


**Figure 3.** Kinetics and time-dependent inhibition of eeAChE by compound **2** (A and C) and compound **3** (B and D). Lineweaver-Burk plot of the eeAChE catalyzed oxidation of ACTI in the absence (control) and presence of various concentrations (2.5  $\mu$ M, 5  $\mu$ M, 10  $\mu$ M) of compound **2** (A) and compound **3** (B). Time-dependent inhibition of AChE catalyzed oxidation of ACTI by compound **2** (C) and compound **3** (D). Rate data are expressed as nmol product formed/min/mg protein. data are the mean  $\pm$  SEM of  $n=3$  determinations.

### Determination of $K_i$ values for lead AChE inhibitors **2** and **3**

The dissociation constant ( $K_i$ ) was calculated to understand the strength of enzyme-inhibitor interaction of lead AChE inhibitor compounds **2** and **3**.  $K_i$  for the lead compounds **2** and **3** were calculated using GraphPadPrism, with a value of  $6.22 \pm 0.002$  nM and  $37.06 \pm 0.014$  nM against eeAChE, respectively. Between the  $IC_{50}$  value and  $K_i$  value obtained for compounds **2** and **3**, an 8-fold and 23-fold difference were observed, suggesting compact binding of the inhibitor to the enzyme.

### Reversibility studies of lead AChE inhibitors **2** and **3**

The most active AChE inhibitors, compounds **2** and **3**, were further examined for time-dependent inhibition studies to understand the reversible/irreversible nature of enzyme inhibition. As depicted in **Fig 3C** and **Fig 3D**, there was no time-dependent decrement in the rates of AChE-catalysed hydrolysis of acetylthiocholine iodide (ACTI) when both the compounds were pre-incubated with AChE for various periods of time (0, 15, 30 and 60 min). From this observation, it can be concluded that AChE inhibition by both the leads is reversible in nature, at least over 60 a min time period. An increase in the AChE catalytic rates with increased pre-incubation times of both the compounds were observed with the enzyme.

### Molecular docking studies of ChE inhibitors

To understand the binding orientation of the inhibitors, molecular docking studies were performed using AutoDock 4.2. The X-ray crystal structures of the recombinant human AChE (PDB code: 4EY7) and human BChE (PDB code: 5DYW) were taken from the Protein Data Bank. The PDB assessment criteria were used to screen a total of more than 200 structures to select the appropriate PDBs (Bound configurations) of the ChEs<sup>[27]</sup>. Iterative gold standard pose (GSP) analysis was performed in the cross-validation of docking poses, where troubleshooting was performed in alienating problematic structures as in the case of BChE structure. The docking results for AChE and BChE were expressed in terms of theoretical inhibition constants ( $K_i$  values) and estimated free energies of binding ( $\Delta G$ ) for each virtual enzyme-inhibitor complex.

### Pose analysis of AChE inhibitors

Examination of the computationally docked binding poses of all the compounds within the AChE active site resulted in the following observations: All the test set of inhibitors were observed to fit well into the active site gorge of AChE formed by the catalytic anionic site (CAS) and the peripheral anionic site (PAS) and were enclosed by the residues: Trp236, Gly121, Asp74, Gly122, Ser125, Tyr124, Leu289, Trp286, Tyr341, Arg296, Phe297, Phe338, Tyr341 and His447. In all the test inhibitors the (methylenedioxy)phenyl moiety binds to the catalytic anionic site, while the variable isatin template binds to the peripheral anionic site. This reveals that almost all the test inhibitors exhibit a completely reverse orientation as the reference drug Donepezil, except in the case of compounds **2** and **6**, which followed similar binding pose as compared to donepezil. Further, these inhibitors are stabilized by hydrogen bonding and hydrophobic ( $\pi$ -alkyl) interactions as shown in **Fig 4A** and **Fig 4B**.

Almost all the compounds were shown to undergo hydrogen bonding interaction with the residues Phe295, Phe296, Gly122, Gly121, Ala204, Asp74, Ser203, and His447. The residue Phe295 is common in all the compounds undergoing hydrogen bonding. Compound **1** formed hydrogen bonding with the residues Phe295 and Arg296; compound **2** formed hydrogen bonding interactions with Asp74 and Phe295; residues Phe295, Gly122, Gly121 and Ala204 formed hydrogen bonding with compound **3**; compound **4** was involved in hydrogen bond formation with the residues Phe295 and Tyr124; compound **5** was involved in hydrogen bonding with residues Ser203 and His447; compounds **7**, **8**, and **9** were involved in hydrogen bonding with common residues Phe295 and Ser203, with the exception of two extra interactions with the residues His447 in the case of compound **8** and Asp74 in the case of compound **9**; compound **10** with the residues Phe295, Tyr124 and His447.

In addition, all the compounds showed hydrophobic ( $\pi$ -alkyl and  $\pi$ -sigma) interactions with the residues Trp286, Leu289, Tyr124, Tyr341, Arg296, Val294, Phe338, Tyr337, and Tyr124. The leads discovered in the study compounds **2** and **3** were shown to undergo hydrophobic  $\pi$ -sigma interactions with Val294, Phe338 and Tyr337, and Trp286 respectively as shown in **Fig 4D**; compound **3** was also involved in  $\pi$ -alkyl interactions with the residues Leu289, Tyr341, Tyr124, and Arg296.

### Binding mode of lead AChE inhibitor compound **2**

Assessment of the virtual complex of the lead AChE inhibitor compound **2** and AChE reveals that the (methylenedioxy)phenyl moiety was bound to the gorge forming the PAS while the variable isatin ring occupies the CAS. The hydrazone linker was found situated in the middle of the gorge between CAS and PAS. The phenyl ring associated with the dioxole ring was found to be interacting with Val294 residue via  $\pi$ -sigma hydrophobic interactions at an inter-planar distance of approximately 3.89 Å. The phenyl ring associated with the isatin template formed  $\pi$ -sigma hydrophobic interactions with the residues Tyr337 and Phe338 at an inter-planar distance of approximately 3.5 Å and 3.4 Å respectively. The oxygen atom present in the carbimino terminal was involved in hydrogen bonding interaction with Phe295 at an inter-planar distance of approximately 2.0 Å. Additionally, the nitrogen atom in the isatin scaffold interacted with the residue Asp74 via hydrogen bonding at an inter-planar distance of approximately 2.1 Å. Also, van der Waals interaction was also observed between the isatin ring and Tyr124 residue at an inter-planar distance of approximately 2.9 Å.

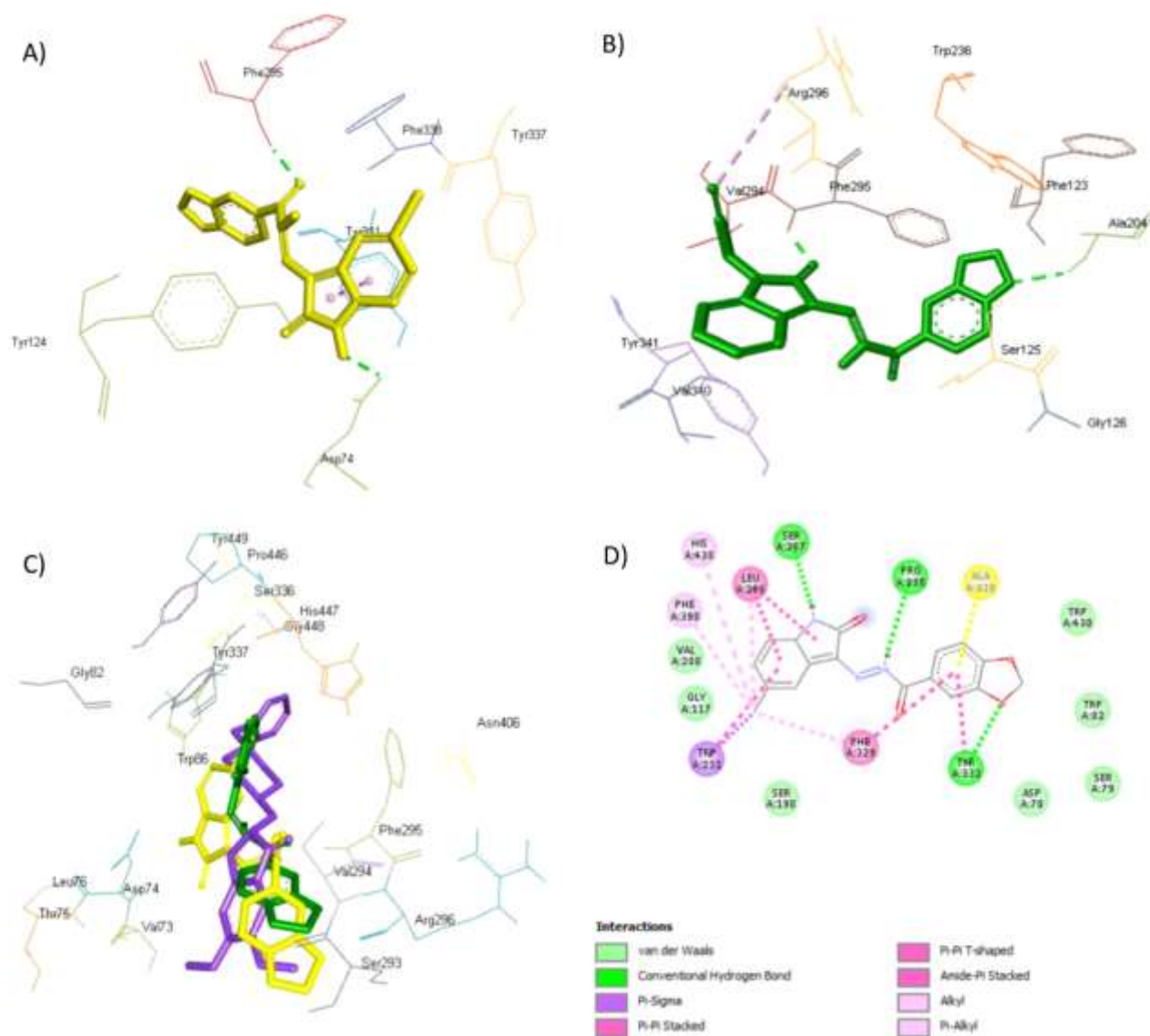


**Figure 4.** A) The binding orientation of compound **2** (yellow in color) in the AChE active site, showing hydrophobic interactions (pink dashed lines) and hydrogen bonding (green dashed line). B) The binding orientation of lead inhibitor compound **3** (green color) showing hydrophobic interactions (pink dashed lines) and hydrogen bonding (green dashed line) with the residues lining PAS and CAS of AChE gorge. C) The superimposed orientation of compound **2** (yellow in color), compound **3** (shown in green), and Donepezil (depicted in purple color) in the AChE active site. D) 2-D interactions displayed by compound **2** in the AChE active site with the aromatic amino acid residues.

### Pose analysis of BChE inhibitors

Examination of the docked poses of all the compounds within the BChE active site resulted in the following observations: All the test inhibitors were found to fit into the gorge of BChE formed by the catalytic anionic site (CAS) and peripheral anionic site and were surrounded by the residues Gly116, Gly117, Ser198, Ala199, Pro285, Val288, Leu286, Ser287, Ala328, Phe329, Tyr332, Phe398, Trp430,

Met437, Tyr440, and His438. The orientation of the compounds was similar to that of the reference inhibitor tacrine when docked with the model.

The compounds **1- 10** were found to be stabilized by hydrogen bonding and  $\pi$ -  $\pi$  interactions. Hydrogen bonding interactions were mainly observed with the residues Gly 116 and Ser 198 in the case of compound **7**; Pro285, Ser117 and Tyr332 residues for compound **1**; Pro285, Ser287 and Tyr332 residues for compound **2**; Ser198 and Gly116 for compound **3**; His438 and Gly117 for compound **4**; Pro285, His438 and Ser287 for compound **5**; Gly116 and Ser198 for compound **7**; Trp82, Trp430 and His438 for compound **9**; Gly78 and Trp430 for compound **10**. Apart from this,  $\pi$ -  $\pi$  interactions rise to be the most prevalent in these compounds with the compound **2** showing  $\pi$ -  $\pi$  interactions with the residues His438, Phe398, Leu286, Ala328 and Phe329 as shown in **Fig 5A**; compound **4** with the residues Trp231, Leu286, Phe329, Ala328, Tyr332 and Trp82; compound **5** with Trp231, Ala328, Tyr332 and Val288; compound **7** with Ala328, Trp82, Trp231, Phe329 and Leu286; compound **9** with Ala328, Met437, Tyr332, Pro285 and Phe329; compound **10** with the residues Ala328, Phe329, Tyr332 and Leu125.

### Binding mode of lead BChE inhibitor compound **3**

Assessment of the virtual complex between the lead inhibitor compound **3** and BChE revealed that compound **3** could perfectly occupy the gorge of BChE simultaneously interacting with the CAS and PAS of BChE as depicted in **Fig 5B**. The N-substituted isatin template was observed to bind to the PAS while the (methylenedioxy)phenyl moiety occupied the CAS, whereas the hydrazone spacer occupied the middle of the gorge between CAS and PAS. The complex was stabilized by hydrogen bonding and  $\pi$ -  $\pi$  interactions where the phenyl part of the (methylenedioxy)phenyl moiety was involved in  $\pi$ -  $\pi$  interactions with the residues Leu286, Phe329, Trp231, and Gly116. The phenyl ring of the isatin template was involved in  $\pi$ -  $\pi$  interactions with the residues Ala328 and Trp82, where the propargyl substitution at the N-position of isatin moiety interacted with Trp82 via  $\pi$ alkyl interaction at an inter-planar distance of approximately 4.7 Å. The oxygen present in the isatin ring was involved in hydrogen bonding with the residue Gly116 at an inter-planar distance of approximately 3.0 Å. The NH present in the carbimino terminal was observed to undergo hydrogen bonding formation with Ser198 at an inter-planar distance of approximately 1.7 Å. The oxygen present in the carbimino terminal underwent hydrogen bonding with Ser198 residue at an inter-planar distance of approximately 2.4 Å. Like as in the case of the AChE model, the BChE binding site interactions were similarly ordered, as in the case of the standard inhibitors.



The tested compounds showed moderate to excellent range in terms of  $IC_{50}$  values, which is in the micromolar range, and also indicated that most of them were selective to the MAO-B enzyme. The  $IC_{50}$  values ranged from  $1.73 \pm 0.087 \mu\text{M}$  (compound **3**) to  $11.2 \pm 0.276 \mu\text{M}$  (compound **8**) for rat MAO-A (rMAO-A), and from  $0.034 \pm 0.007 \mu\text{M}$  (compound **3**) to  $4.13 \pm 0.092 \mu\text{M}$  (compound **7**) for rMAO-B. Among the tested compounds, compound **3** was identified as the most active MAO-A inhibitor, with  $IC_{50}$  values of  $1.73 \pm 0.087 \mu\text{M}$ , as well as the most active MAO-B inhibitor, where the  $IC_{50}$  value was found to be  $0.034 \pm 0.007 \mu\text{M}$ . It was also observed that compound **3** was 50 folds more selective towards MAO-B enzyme than MAO-A, and the inhibitory potential for MAO-B isozyme was close to that of the reference standard Selegiline. The second best MAO-A inhibition profile was observed in the case of compound **10**, which displayed an  $IC_{50}$  value of  $1.97 \pm 0.018 \mu\text{M}$ , followed by compound **4**. In the case of MAO-B, compound **8** was observed to have the second best activity, with an  $IC_{50}$  value of  $0.52 \pm 0.093 \mu\text{M}$ , followed by compound **4**, which showed an  $IC_{50}$  value of  $0.546 \pm 0.032 \mu\text{M}$ . From the inhibitory data produced in **Table 3**, SAR has been derived for the tested compounds.

### SAR for MAO-A inhibition

The ortho and para-substituted dichloro benzyl group in the  $R_1$  position of the isatin ring gave rise to better MAO-A activity, as in the case of compound **10** than the para-substituted fluoro benzyl derivative, compound **8**, and benzyl substituted derivative, compound **7**. The substitution with para-fluoro benzyl group at the  $R_1$  position, compound **8**, led to a drastic decrease in the activity as compared to the benzyl substituted derivatives. The aliphatic side chain substitution at  $R_1$  position by propargyl and allyl group compounds **3** and **4** respectively, led to an increase in activity, thereby showing better results than that of the benzyl-substituted derivatives, except in the case of compound **10**, which showed comparable results as to that of compound **4**. Substitution at the  $R_2$  position by a chlorine group led to a decrease in the MAO-A activity as compared to the  $R_1$  substituted compounds, except in the case of compound **8**, which showed the lowest activity among the tested compounds. Compound **3** was shown to possess overall better MAO-A inhibitory activity than the rest of the test series.

**Table 3.** *In vitro* and computational results of MAO inhibition studies for compounds **1-10**.

Compd	MAO-A	MAO-B
-------	-------	-------

	IC <sub>50</sub> [ $\mu$ M] <sup>[a]</sup>	$\Delta$ G [kcal mol <sup>-1</sup> ] <sup>[b]</sup>	Ki [ $\mu$ M] <sup>[b]</sup>	IC <sub>50</sub> [ $\mu$ M] <sup>[a]</sup>	$\Delta$ G [kcal mol <sup>-1</sup> ] <sup>[b]</sup>	Ki [ $\mu$ M] <sup>[b]</sup>
<b>1</b>	-	-7.96	-	-	-10.02	-
<b>2</b>	5.164 $\pm$ 0.131	-7.57	1.56	0.89 $\pm$ 0.096	-10.4	0.17
<b>3</b>	1.73 $\pm$ 0.087	-5.86	45.76	0.034 $\pm$ 0.007	-10.65	0.019
<b>4</b>	2.51 $\pm$ 0.058	-5.92	31.45	0.546 $\pm$ 0.032	-10.55	0.217
<b>5</b>	-	-6.27	16.34	-	-10.78	-
<b>6</b>	-	-6.45	9.86	-	-10.55	-
<b>7</b>	3.46 $\pm$ 0.009	-5.32	120.56	4.13 $\pm$ 0.092	-12.25	1.19
<b>8</b>	11.2 $\pm$ 0.276	-5.28	142.76	0.52 $\pm$ 0.093	-12.15	0.046
<b>9</b>	-	-5.89	36.32	-	-12.32	-
<b>10</b>	1.97 $\pm$ 0.018	-5.25	136.37	0.64 $\pm$ 0.072	-10.96	0.325
<b>CLR</b>	0.0043 $\pm$ 0.008	-	-	-	-	-
<b>SGL</b>	-	-	-	0.02 $\pm$ 0.0045	-	-

<sup>[a]</sup> Each IC<sub>50</sub> value is the mean  $\pm$  SEM. Level of statistical significance:  $p < .05$  versus the corresponding IC<sub>50</sub> values obtained against MAO's, as determined by ANOVA/Dunnett's. Reference inhibitors: CLR– Clorgyline, SGL - Selegiline. <sup>[b]</sup> Computationally predicted values.

### SAR for MAO-B inhibition

Substitution at R<sub>1</sub> position by para-substituted fluoro or dichloro substituted benzyl groups, compounds **8** and **10** respectively, led to an increase in MAO-B inhibitory activity as compared to the unsubstituted benzyl derivative, compound **7**. Compounds **8** and **10** displayed, respectively, 22-fold and 3-fold selectivity than MAO-A, while compound **7** was the least selective of the tested compounds. Aliphatic side chain substitution at R<sub>1</sub> position by propargyl and allyl group led to an increase in activity as compared to the benzyl-substituted compounds, except in the case of a para-fluoro substituted benzyl group, compound **8**, where it was shown to have comparable activity to that of the allyl-substituted derivative, compound **4**. The substitution at R<sub>2</sub> position by a chloro group, in compound **2**, did not show any substantial increase in activity but was shown to possess better selectivity and activity than compound **7**. Compound **3**, with propargyl substitution at the R<sub>1</sub> position, was shown to have the highest MAO-B inhibitory activity and selectivity (more than 50 fold as compared to MAO-A) among the tested compounds.

### Kinetic studies of lead MAO-B inhibitor **2** and **3**

The inhibition mode of the discovered lead MAO-B inhibitors, **2** and **3**, was examined by performing Lineweaver-Burk plots. The plots obtained for compound **2** (**Fig 6A**) showed increased slopes (decreased  $V_{\max}$ ), which intercepted (higher  $K_m$ ) at increasing concentration of the inhibitors. This implies a mixed-type inhibition by compound **2** and consequently support the dual site binding property of the compound<sup>[32]</sup>. The Lineweaver-Burk plot for Compound **3** (**Fig 6B**) was linear and intersected at the Y-axis. This pattern showed that compound **3** inhibited MAO-B competitively, and further extrapolation of the results proved that they bind reversibly to MAO-B.

### Determination of $K_i$ value for lead MAO-B inhibitor compound **3**

The dissociation constant ( $K_i$ ) was calculated using GraphPad Prism software to determine the strength of enzyme-inhibitor interaction of lead MAO-B inhibitor, compound **3**.  $K_i$  value for competitive inhibitor **3** was calculated to be  $12.14 \pm 0.026$  nM against rMAO. Between the  $IC_{50}$  value and  $K_i$  value obtained for compound **3**, approximately a 3-fold difference was observed, suggesting compact binding of the inhibitor to the enzyme.

### Reversibility studies of lead MAO-B inhibitor compounds **2** and **3**

The lead MAO-B inhibitors **2** and **3** were further tested for time-dependent inhibition studies to determine whether the inhibition was reversible or irreversible. The reversibility test was performed by adopting a slightly modified method as described by Legoabe et al<sup>[33]</sup>. There was no time-dependent decrease in the rates of rMAO-B catalyzed the oxidation of benzylamine when compound **2** (**Fig 6C**) and **3** (**Fig 6D**) were pre-incubated with the enzyme for various time intervals (0, 15, 30, and 60 min). From these results, it was concluded that inhibition of rMAO-B by both **2** and **3**, was reversible, at least within a 60 min time period. An increase in rMAO-B catalytic rates was also observed owing to prolonged incubation times with both compounds.

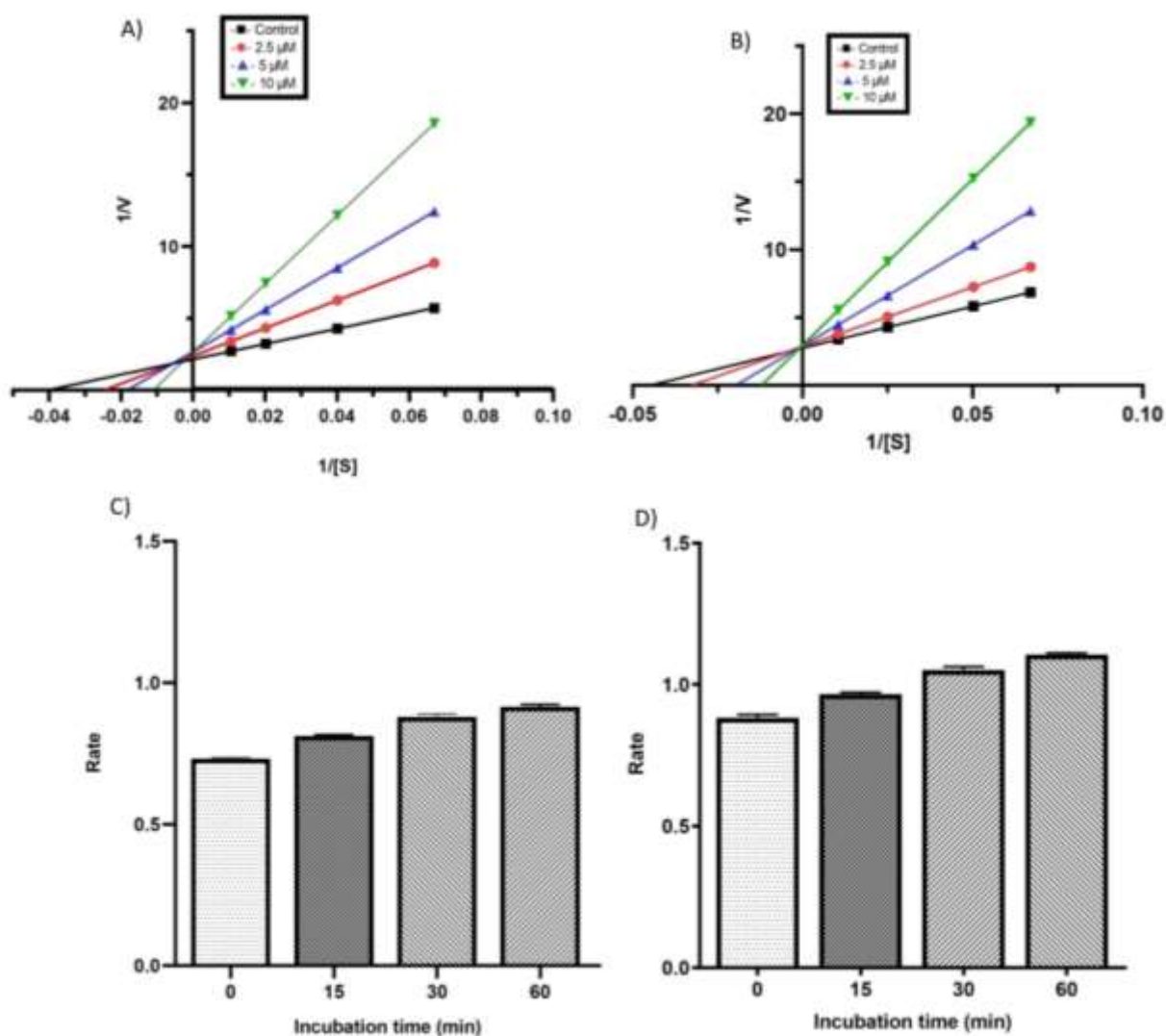


**Figure 6.** Kinetics and time-dependent inhibition of rMAO-B by compound **2** (A and C) and compound **3** (B and D). Lineweaver-Burk plot of the MAO-B catalyzed oxidation of benzylamine in the absence (control) and presence of various concentrations (2.5  $\mu\text{M}$ , 5  $\mu\text{M}$ , 10  $\mu\text{M}$ ) of compound **2** (A) and compound **3** (B). Time-dependent inhibition of AChE catalyzed oxidation of benzylamine by compound **2** (C) and compound **3** (D). Rate data are expressed as nmol product formed/min/mg protein. data are the mean  $\pm$  SEM of  $n=3$  determinations.

### Molecular modeling studies of MAO inhibitors

The Gold Standard Pose (GSP) of the co-crystallized bound protein-ligand complex was produced to validate the docking procedure, and for the study, hMAO-A, and hMAO-B were procured from the RCSB PDB database.

According to the PDB analysis criteria adapted for the selection of the appropriate PDB structures for the modeling studies<sup>[27]</sup>, human MAO-A (PDB code: 2Z5X) and human MAO-B (PDB code: 2V5Z)

were selected. The selection was performed out of a test set of more than 40 structures, in the case of MAO-B structures and around 5 structures for MAO-A structures (containing both bound and unbound structures). The GSP was determined to create precision and validate the structure of selected structures, which was also a major part of the screening analysis for the selection of the appropriate PDB structure. In cases where the GSP was hard to achieve, structures with Root Mean Square Deviation (RMSD)  $< 2.0 \text{ \AA}$ , the next in line of the most suitable models were chosen to undergo the validation studies, as what happened in the case of MAO-A enzyme. The results of the docking studies were expressed theoretically as binding free energies ( $\Delta G$ ) and inhibition constants ( $K_i$  values) for each of the ligand-protein complex and are presented in **Table 3**.

### Binding pose analysis of MAO-A inhibitors

Evaluation of virtual ligand-protein complexes of all the compounds **1-10** within the catalytic site of MAO-A resulted in the below-mentioned interpretations: All the tested compounds occupied the active site cavity of MAO-A and were framed within the binding pocket surrounded by the amino acid residues Ile180, Asn181, Phe208, Val210, Gln215, Ile325, Tyr407, Tyr444 and FAD which was almost similar to the reference MAO-A inhibitor, harmine. Compounds **2** and **4** were grouped with the reference inhibitor to get the pose, where similar binding orientation was observed within the active site of MAO-A.

In all the compounds, the (methylenedioxy)phenyl ring occupies the space extending towards the cavity while the variable isatin group is located towards FAD. Further, the inhibitors are stabilized by hydrophobic  $\pi$ -alkyl and  $\pi$ - $\pi$  stacked interactions. None of the selected compounds showed an inclination for hydrogen bond formation, where the main  $\pi$ - $\pi$  alkyl interactions were observed with the residues Phe208, Ile180, Ile335, Leu337, FAD and Tyr444, while  $\pi$ - $\pi$  stacked interactions were observed between the residues Tyr407 and Phe352. The  $\pi$ -sigma interactions were mainly common with one residue Gln215 with the (methylenedioxy)phenyl moiety of the molecule. Compound **3** was observed to show  $\pi$ -alkyl interactions, from the propargyl group of the parent to the amino acid residues Phe208 and Ile180 as shown in **Fig 7A** and **Fig 7B**. The isatin moiety was shown to take part in the majority of the hydrophobic interactions, thus stabilizing inside, near the FAD pocket. Thus in the more potent compound, preferably  $\pi$ -alkyl and  $\pi$ - $\pi$  interactions have been found to be responsible for mediating the inhibitory activity against MAO-A.



case of reference MAO-B inhibitor, safinamide. The majority of the test inhibitors showed the same orientations towards the binding pocket. The amide functional side chain of the safinamide inhibitor was oriented towards the FAD molecule and the fluoro benzyl group was observed to position towards the opening of the cavity. The compounds **1-8** possessed similar orientation where the variable isatin moiety was headed towards the FAD and the (methylenedioxy)phenyl group was positioned towards the cavity opening. Only compound **10** proved to be an exception where the orientation is reversed completely. The inhibitors are stabilized by hydrogen bonding and  $\pi$ -alkyl interactions.

All the compounds showed hydrogen bonding interactions with the target residues mainly Ile199, Tyr326, Gln206, Ile198, Tyr435, Tyr188 and Cys172. The compound **1** and **2** showed hydrogen bonding interactions with the residues Gln206 and Tyr435, while compound **3** showed hydrogen bonding with residues Ile199, Tyr326, Gln206 and Ile198. Compound **4** and **6** showed hydrogen bonding with the common residue Gln206, with compound **4** showing extra interaction with Ile198. The hydrogen bonding interactions expressed by compound **5** with Tyr188 and Cys172 stands out as uncommon among the other compounds. The residues Gln206, Cys172 and Ile198 displayed hydrogen bonding interactions with compound **7**. The compounds compound **8** and **9** showed similar hydrogen bonding interactions with residues Gln206 and Ile198, while compound **10** displayed interactions with Cys172 and Ile198 residues of the enzyme. Additionally,  $\pi$ -alkyl interactions were shown by all the compounds, the active residues namely: Cys172, Tyr60 and Tyr435 in the case of compound **3**, the most active inhibitor from the series. In the study, it was concluded that in most of the potent compounds preferably  $\pi$ -alkyl and hydrogen bonding interactions are responsible for mediating inhibition against MAO-B.

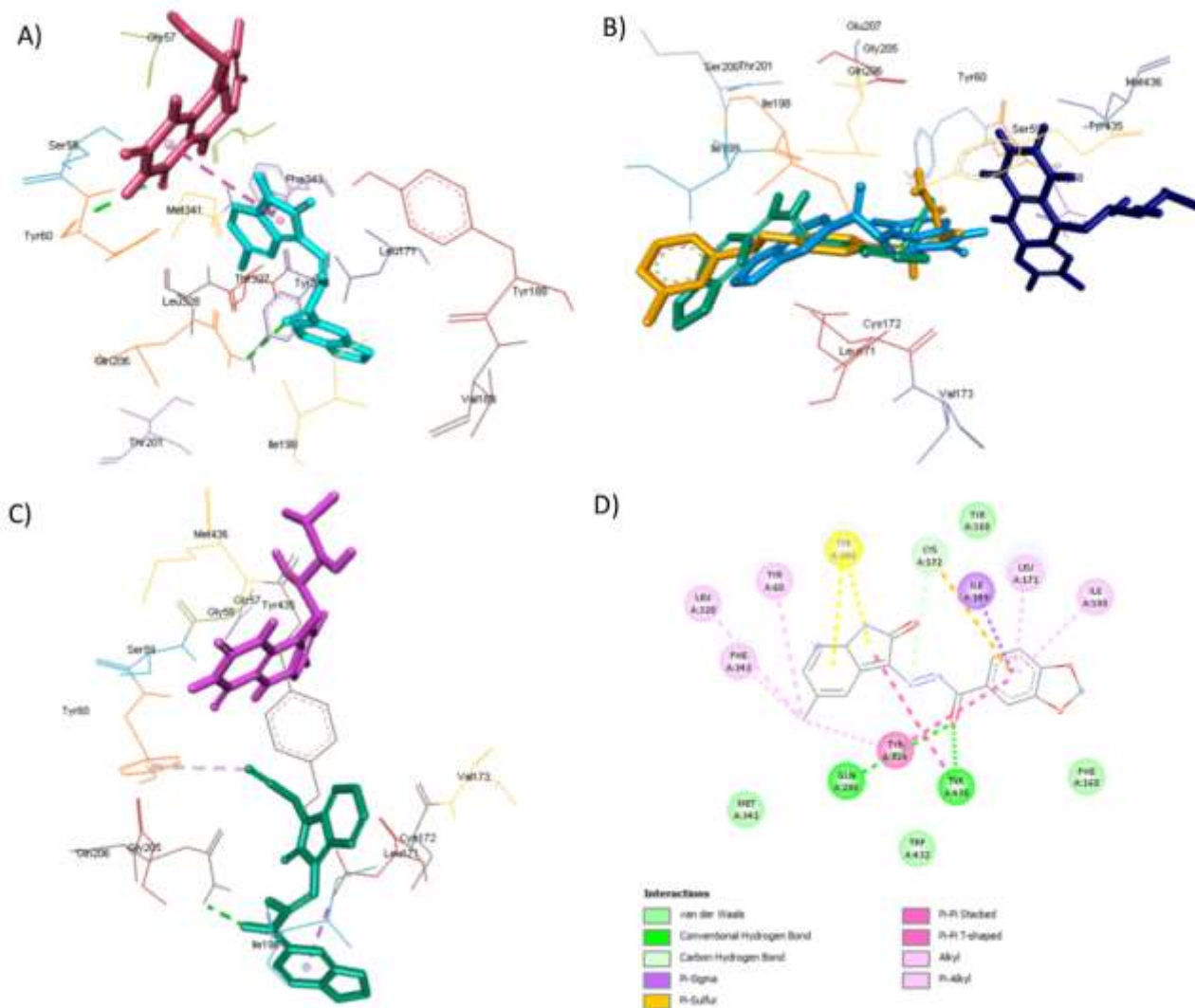


**Figure 8.** A) The binding orientation of compound **2** (blue) in the active site cavity of MAO-B enzyme along with the co-factor FAD (purple), showing important hydrophobic (pink dashed line) and hydrogen bonding (green dashed line) interactions. B) The superimposed orientation of compound **2** (blue), compound **3** (green), and safinamide (yellow) in the active site cavity of MAO-B enzyme along with the co-factor FAD (dark blue). C) The binding orientation displayed by compound **3** (green) with the amino acid residues within the active site and FAD (violet). D) The 2-D interactions observed in one of the lead MAO-B inhibitor, compound **2**, with the aromatic residues lining the active site.

### Binding mode of lead MAO-B inhibitor compound **3**

Study of the lead MAO-B inhibitor, compound **3**, reveals that the entire molecule is stabilized in both the cavities with the rigid (methylenedioxy)phenyl moiety extending towards the entrance cavity of MAO-B, while the variable isatin group is caged into the substrate cavity as displayed in **Fig 8C**. The compound is found to exhibit a  $\pi$ -alkyl interaction between propargyl group of the side chain in the isatin moiety and Tyr60 residue at an inter-planar distance of approximately 4.73 Å. The isatin

template showed  $\pi$ -sigma and  $\pi$ -alkyl interactions with the residues Leu171, and Tyr435, Cys172 and Tyr398 respectively at an interplanar distance of approximately 4.3 Å, 5.4 Å, 5.0 Å, and 5.3 Å respectively. In addition, hydrogen bonding interactions were observed between the oxygen of the carbimino linker and Tyr326, Ile199 and Gln206 with an inter-planar distance of 2.9 Å, 2.7 Å and 2.4 Å respectively. Additional hydrogen bonding interactions were observed between the nitrogen involved in the carbimino bond with the residue Ile198 at an inter-planar distance of 2.2 Å. These interactions in tandem resulted in the firmness of the ligand within the MAO-B active site cavity and hence confirm the stability of the complex. In most of the compounds, it was seen that the variable hydrophobic isatin region was involved in strong hydrophobic interactions with the FAD molecule, as in the case of the standard inhibitor as shown in **Fig 8D**.

**Table 4.** Drug-Likeness and Pharmacokinetic properties of compounds **1-10**.

Properties	1	2	3	4	5	6	7	8	9	10
<b>Drug Likeness</b>										
-Lipinski Rule of 5	pass									
<b>Absorption</b>										
-WS (log molL <sup>-1</sup> )	-3.403	-3.446	-3.682	-3.943	-3.569	-3.499	-5.268	-4.957	-5.186	-5.155
-IA (%)	91.82	92.12	95.68	95.25	83.99	92.05	93.70	93.37	91.45	92.5
-SP (log K <sub>p</sub> )	-2.907	-3.003	-3.262	-2.802	-2.795	-3.002	-2.76	-2.74	-2.741	-2.742
<b>Distribution</b>										
-BBBP (log BB)	-0.083	-0.433	-0.262	-0.288	-0.745	-0.442	-0.231	-0.335	-0.441	-0.508
-CNSP (log PS)	-2.407	-2.342	-2.462	-2.506	-2.575	-2.319	-2.178	-2.224	-1.944	-2.19
<b>Metabolism</b>										
-CYP3A4 inhibitor	No	No	No	No	No	No	Yes	Yes	Yes	Yes
-CYP2C9 inhibitor	No									
<b>Excretion</b>										
-TC (log ml/min/Kg)	0.098	-0.325	0.264	0.36	0.375	-0.347	0.205	-0.055	-0.292	-0.479
<b>Toxicity</b>										
AMES toxicity	No	Yes	Yes	Yes	Yes	Yes	No	Yes	Yes	Yes
MTD (log mol/Kg/day)	-0.346	-0.026	-0.366	-0.059	-0.257	-0.035	-0.319	-0.451	-0.493	-0.387
ORAT (mol/Kg)	1.962	1.957	2.524	2.499	2.422	1.969	2.681	2.452	2.531	2.492
HT	No	No	No	Yes	Yes	No	Yes	Yes	Yes	Yes
SS	No									
CT	No									

\*Abbreviations: LLR = Lead Like Rule, WS = Water Solubility, IA = Intestinal Permeability, SP = Skin Permeability, BBBP = Blood Brain Barrier Permeability, CNSP = Central Nervous System Permeability, TC = Total clearance, MTD = Maximum Tolerated Dose, ORAT = Oral Rat Acute Toxicity, HT = Hepatotoxicity, SS = Skin Sensitization, CT = Cytotoxicity.

### ***In silico* drug-likeness and pharmacokinetic prediction**

The *in silico* pharmacokinetic properties were determined for all the compounds using online pkCSM server and ProTox server<sup>[29,30]</sup>. All the compounds showed high water solubility within the range of -5.268 (log molL<sup>-1</sup>), in case of compound 7, to -3.403 (log molL<sup>-1</sup>), for compound 1. Intestinal absorption (IA) was found to be greater than 90% for all the tested compounds except for compound 5, which was shown to have 83% absorption. Compound 3 had the highest IA of 95.68% followed by compound 4 with 95.25%. All the compounds were skin permeable, showing a range from -3.262 (log K<sub>p</sub>), as observed for compound 3, to -2.74 (log K<sub>p</sub>), calculated for compound 8. Compounds 1-10 have the potential to cross the blood-brain barrier (BBB) and exhibit range from -0.745 (log BB), for compound 5, to -0.083 (log BB), for compound 1. The CNS permeability values for all the compounds were found to be greater than -2.60 (log PS), with compound 9 displaying the highest value of -1.944, pertaining to greater penetration into the CNS. The compounds 1-6 are identified to be non-inhibitors of the metabolizing enzyme CYP3A4, while compounds 7-10 inhibit the enzyme and can potentially stop the metabolism of xenobiotic agents. All the compounds, 1-10, also did not inhibit the CYP2C9. The compounds 1-10 showed Total Clearance between -0.429 (log ml/min/Kg) for compound 10 and 0.375 (log ml/min/Kg) as in the case of compound 5. Compounds 1 and 7 gave a negative response to the AMES test, while the rest gave positive results. The Maximum Tolerated Dose (MTD) for the compounds 2 and 6 were predicted to be -0.026 (log mol/Kg/day) and -0.035 respectively. The Oral Rat Acute Toxicity (ORAT) model predicted values of 1.957 mol/kg and 2.524 mol/kg for compounds 2 and 3 respectively. Compounds 4, 5 and 7-10 were hepatotoxic in nature, while compounds 1-3 and 6 were shown to be non-hepatotoxic. None of the compounds were predicted to be skin sensitive and cytotoxic in nature. All the results of pharmacokinetic predictions are presented in **Table 4**.

### **Conclusion**

The application of hydrazones has spread extensively in targeting new pathophysiological conditions with the development of efficient synthetic methodologies. In the present work, we attempted to identify new MTDLs with dual MAO and ChE inhibitory properties. To bring full justice to the study, we designed and synthesized a series of piperonylic acid derived hydrazones containing isatin scaffold

with varying degree of steric and electronic features (compounds **1-10**) based on the MTDL approach and evaluated their pharmacological profile through virtual molecular docking and enzymatic screening assays (in vitro MAO and ChE inhibition assays) respectively. In silico molecular property analysis and ADMET, prediction studies were also carried out to predict the pharmacokinetic profile of the compounds. From the preliminary in vitro MAO and ChE inhibition studies, we have identified two lead molecules, compounds **2** and **3**, from the series possessing dual inhibition potential against both the enzymes. Most of the compounds were found to be more selective towards MAO-B isozyme than MAO-A, especially in the case of compound **3**, where it was shown to have more than 50 folds more selectivity towards MAO-B isozyme. Additional Kinetic and reversibility/irreversibility studies were performed for the lead inhibitors of the study, compounds **2** and **3**, to understand the type and strength of enzyme-inhibitor binding. Compound **2** displayed competitive inhibition for AChE (lead inhibitor) and a mixed type inhibition for MAO-B, thereby supporting our dual site binding model. It was also identified to undergo reversible inhibition with both AChE and MAO-B respectively. Compound **3** was identified as a competitive as well as a reversible inhibitor of MAO-B isozyme as well as AChE.

The identified leads were found to be more potent than the previously discovered lead compound **22**, whose MAO-B and MAO-A inhibition  $IC_{50}$  values were  $7.253 \pm 0.002 \mu\text{M}$  and  $16.40 \pm 0.011 \mu\text{M}$  respectively. On comparing the hydrazone lead compound **3** to the semicarbazone based compound **22**<sup>[25]</sup> from our earlier study, it was observed that the removal of NH group attached to the (methylenedioxy)phenyl moiety led to an increase in overall activity and selectivity towards MAO-B enzyme as shown in **Fig 9**. Also, the docking analysis revealed strong hydrophobic interactions governing the stability of compound **3** in the active site pocket as compared to compound **22**.

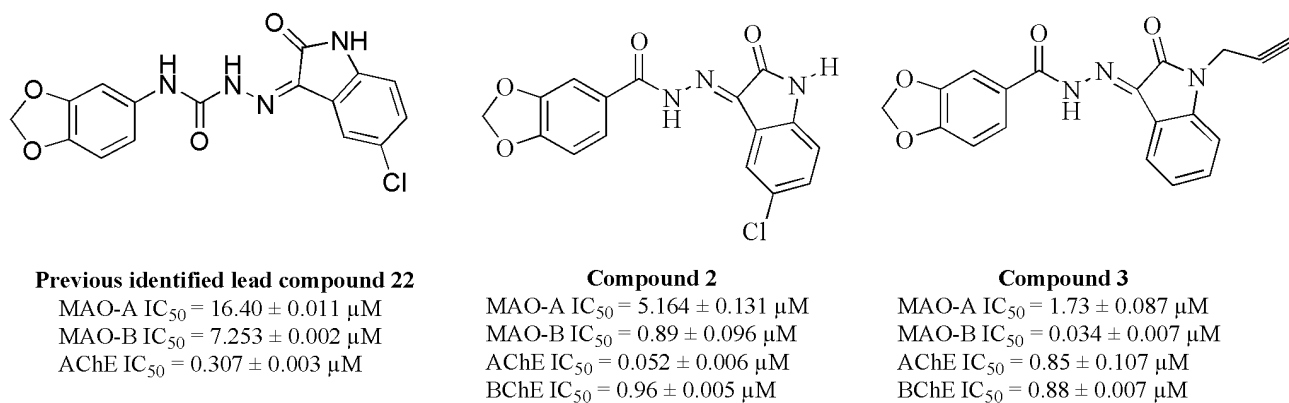


**Figure 9.** The MAO/ChE inhibition data ( $IC_{50}$ ) for present lead compounds **2** and **3**, along with earlier developed compound **22**.

Most of the compounds of the hydrazone series were found to be potent inhibitors of AChE enzyme, with the exception of compound **5**. The lead AChE inhibitors obtained from the study are compound **2** and **3**, while compound **3** emerged as the best BChE inhibitor. The identified leads were found to be more potent than the previous lead discovered compound **22**<sup>[25]</sup>, whose AChE IC<sub>50</sub> value was 0.307 ± 0.003 μM. On comparing the hydrazone lead compound **2** to the semicarbazone based compound **22**, it was observed that the removal of the hydrogen-bond donor, NH group associated with the (methylenedioxy)phenyl moiety led to an increase in overall activity towards AChE enzyme.

The docking results confirmed stronger hydrophobic interactions with the active site gorge for compound **3** relative to the semicarbazone-isatin leads previously developed.

The present work yielded some lead MAO and ChE inhibitors with interesting activity profile. The truncation of the semicarbazino linker into a hydrazone linker has yielded far more potent compounds with superior IC<sub>50</sub> values in the case of AChE and MAO-B inhibition, with greater selectivity towards MAO-B. Compound **2** (N'- [(3E)- 5- chloro- 2- oxo- 2,3- dihydro- 1H- indol- 3- ylidene]- 2H- 1,3- benzodioxole- 5- carbohydrazide) and compound **3** (N'-(2-oxo-1-(prop-2-ynyl)indolin-3-ylidene)benzo[d][1,3]dioxole-5-carbohydrazide) have emerged as the most promising dual acting lead compounds which warrant further optimization and preclinical development as neurotherapeutic agents.

## Experimental Section

The specific reactant materials and reagents were procured from Alfa Aesar and Merck (Sigma-Aldrich) and were consumed without further purification. Melting points (mp) were mapped using a one-end-closed capillary tube on a Systronics digital melting point apparatus (model IIC327) and are uncorrected. IR spectra were recorded on an Alpha II Infrared Spectrometer (FT-IR, Bruker) by means of potassium bromide disc method. <sup>1</sup>H and <sup>13</sup>C were recorded on a Bruker 500 MHz High-Resolution FT NMR Spectrophotometer at ambient temperature using deuterated DMSO ([D<sub>6</sub>] DMSO) as a solvent. Chemical shifts are expressed as δ units (ppm) relative to TMS. All exchangeable protons were confirmed by addition of D<sub>2</sub>O. Spin multiplicities are expressed as s (singlet), d (doublet), t (triplet), dd (doublet of doublet), or m (multiplet). Coupling constants (J) are expressed in hertz (Hz). Mass spectra were recorded on a **Waters Xevo TQD triple Quadrupole mass spectrometer**.

Elemental analyses for C, H, and N were determined with a CE-440 CHN analyzer (Exeter Analytical), and the analytical results were within  $\pm 0.4$  % purity for all compounds.

## Intermediates

**Methyl 2H-1,3-benzodioxole-5-carboxylate (I):** 0.027 moles of piperonylic acid was dissolved in 100 ml of methanol in a 250 ml round-bottom flask. To the solution, 0.072 moles of concentrated sulfuric acid (3.83 ml) was added and refluxed at 80 °C for 2 hours (monitored by TLC). The reaction mixture was poured into ice cold water to obtain a white colored crystalline precipitate. The precipitate was filtered out and washed with cold water and vacuum dried. Recrystallization was performed using ethanol (yield: 90%, mass: 180.16 gmol<sup>-1</sup>, R<sub>f</sub>: 0.53, mp: 52-54 °C): <sup>1</sup>H NMR ([D<sub>6</sub>] DMSO):  $\delta$  = 3.76 (s, 3H, CH<sub>3</sub>), 6.17 (s, 2H, benzodioxole C2), 7.03 (d, J = 7.5, 1H, benzodioxole C4), 7.34 (s, 1H, benzodioxole C7), 7.48 (d, J = 8.4, 1H, benzodioxole C5); <sup>13</sup>C NMR ([D<sub>6</sub>] DMSO):  $\delta$  = 52.32 (methyl C), 102.03 (benzodioxole C2), 107.99 (benzodioxole C4), 112.67 (benzodioxole C7), 126.43 (benzodioxole C5), 133.59 (benzodioxole C6), 139.65 (benzodioxole C3a), 141.08 (benzodioxole C7a), 168.31 (C=O); IR (KBr):  $\tilde{\nu}$  = 1413.46 (aromatic C=C med), 1746.12 (C=O str), 1296.76, 1067.22 (C-O str); Anal. for C<sub>9</sub>H<sub>8</sub>O<sub>4</sub>: calcd: C (60.02%), H (4.46%), O (35.52%), found: C (60.08%), H (4.49%), O (35.43%)

**2H-1,3-benzodioxole-5-carbohydrazide (II):** 10ml of hydrazine monohydrate (0.201 mol) was added to a solution of I (0.0201 mol) in ethanol (60ml) while stirring. The solution was refluxed at 80 °C with stirring for 2 hrs (monitored by TLC). After completion of the reaction, the mixture was poured onto ice-cold water to obtain a white crystalline precipitate. The precipitate was filtered and washed with ice cold water. Recrystallisation was performed using ethanol (yield: 86%, mass: 180.16 gmol<sup>-1</sup>, R<sub>f</sub>: 0.38; mp: 170-172 °C): <sup>1</sup>H NMR ([D<sub>6</sub>] DMSO):  $\delta$  = 1.96 (s, 2H, NH<sub>2</sub>), 6.14 (s, 2H, benzodioxole C2), 7.02 (d, J = 8.4, 1H, benzodioxole C4), 7.42 (s, 1H, benzodioxole C7), 7.50 (d, J = 8.3, 1H, benzodioxole C5), 8.02 (s, 1H, NH); <sup>13</sup>C NMR ([D<sub>6</sub>] DMSO):  $\delta$  = 101.90 (benzodioxole C2), 107.43 (benzodioxole C4), 108.23 (benzodioxole C7), 126.56 (benzodioxole C5), 135.12 (benzodioxole C6), 138.45 (benzodioxole C3a), 140.09 (benzodioxole C7a), 165.43 (C=O); IR (KBr):  $\tilde{\nu}$  = 3320.32 (N-H med), 1420.12 (aromatic C=C med), 1679.84 (C=O str), 1276.53, 1046.08 (C-O str); Anal. for C<sub>8</sub>H<sub>8</sub>N<sub>2</sub>O<sub>3</sub>: calcd: C (53.34%), H (4.47%), N (15.57%), O (26.62%), found: C (53.39%), H (4.42%), N (15.60%), O (26.59%)

## Final Products

**General procedure for the conventional synthesis of hydrazones clubbed isatin derivatives:** All the final compounds (5-(un) N-substituted isatinyl hydrazones) were synthesized by the reaction of **II** (0.002 mol) with an equimolar quantity of appropriately substituted isatin derivatives (0.002 mol). Then the pH of the reaction mixture was adjusted to 5-6, using glacial acetic acid, and was stirred at reflux for 2-8 hrs. After the completion of the reaction, the reaction mixture was cooled to room temperature and the precipitated product was filtered and vacuum dried. The precipitate was further washed with ethanol to remove any starting material. The yield of the final compounds 1-10 was obtained between 79- 96%.

**N'-(3E)-2-oxo-2,3-dihydro-1H-indol-3-ylidene]-2H-1,3-benzodioxole-5-**

**carbohydrazide (1):** yield: 94%; mass: 309.07 gmol<sup>-1</sup>; mp: 266-269 °C; R<sub>f</sub>: 0.64; <sup>1</sup>H NMR ([D6] DMSO): δ = 6.16 (s, 2H, benzodioxole C2), 6.91 (dd, J = 8.2, 8.4, 2H, benzodioxole C6, C7), 6.96 (t, J = 8.0, 1H, isatinyl C5), 7.50 (s, 1H, benzodioxole C4), 7.58 (d, J = 8.45, 1H, isatinyl C4), 7.79 (t, J = 7.3, 1H, isatinyl C6), 7.88 (d, J = 7.8, 1H, isatinyl C7), 8.56 (s, 1H, NH), 10.85 (s, 1H, isatinyl NH); <sup>13</sup>C NMR ([D6] DMSO): δ = 102.87 ( benzodioxole C2), 110.56 ( benzodioxole C7), 110.92 ( benzodioxole C4), 113.81 (isatinyl C7), 117.35 (isatinyl C5), 120.22 (isatinyl C3a), 122.54 (benzodioxole C5), 125.62 (isatinyl C6), 128.41 (isatinyl C4), 135.82 (benzodioxole C6), 140.23 (benzodioxole C3a), 140.44 (benzodioxole C7a), 140.53 (isatinyl C7a), 142.42 (isatinyl C3), 164.2 (C=O), 170.3 (isatinyl C=O); IR (KBr): ν̄ = 3214.37 (N-H str), 2981.30 (C-H med), 1417.66 (aromatic C=C med), 1696.51, 1680.69 (C=O str), 1605.62 (C=N str), 1256.99 (C-N str), 1288.95, 1037.91 (C-O str); Anal. for C<sub>16</sub>H<sub>11</sub>N<sub>3</sub>O<sub>4</sub>: calc: C (62.14%), H (3.59%), N (13.58%), O (20.69%), found: C (62.23%), H (3.51%), N (13.50%), O (20.76%)

**N'-(3E)-5-chloro-2-oxo-2,3-dihydro-1H-indol-3-ylidene]-2H-1,3-benzodioxole-**

**5- carbohydrazide (2):** yield: 90.5%; mass: 343.04 gmol<sup>-1</sup>; mp: 286-290 °C; R<sub>f</sub>: 0.72; <sup>1</sup>H NMR ([D6] DMSO): δ = 6.18 (s, 2H, benzodioxole C2), 6.98 (d, J = 8.5, 1H, benzodioxole C7), 7.14 (d, J = 8.3, 1H, benzodioxole C6), 7.38 (s, 1H, isatinyl C4) 7.43 (m, J = 8.6, 9.1, 2H, isatinyl C6, C7), 7.58 (s, 1H, benzodioxole C4), 11.40 (s, 1H, NH), 13.70 (s, 1H, isatinyl NH); <sup>13</sup>C NMR ([D6] DMSO): δ = 102.73 ( benzodioxole C2), 109.13 ( benzodioxole C4, C7) , 113.25 (isatinyl C7), 120.84 (isatinyl C3a), 122.34 ( benzodioxole C5), 126.27 (isatinyl C4), 127.34 (isatinyl C5), 131.55 (isatinyl C6, benzodioxole C6), 141.54 (benzodioxole C3a), 148.53 (benzodioxole C7a), 151.77 (isatinyl C3,

isatinyl C7a), 163.38 (isatinyl C=O, C=O); IR (KBr):  $\tilde{\nu}$  = 3197.67 (N-H med), 2980.67 (C-H med), 1434.91 (aromatic C=C med), 1702.11, 1680.70 (C=O str), 1614.99 (C=N str), 1252.06 (C-N str), 1171.46, 1029.39 (C-O str), 744.87 (C-Cl str); MS:  $m/z$  = 344 [M+1], 346 [M+2]; Anal. for C<sub>16</sub>H<sub>10</sub>ClN<sub>3</sub>O<sub>4</sub>: calcd: C (55.91%), H (2.93%), Cl (10.31%), N (12.23%), O (18.62%), found: C (55.87%), H (2.95%), Cl (10.28%), N (12.34%), O (18.56%)

**N'-(3E)-2-oxo-1-(prop-2-yn-1-yl)-2,3-dihydro-1H-indol-3-ylidene]-2H-1,3-benzodioxole-5-carbohydrazide (3):** yield: 86.5%; mass: 347.32 gmol<sup>-1</sup>; mp: 190-195 °C; R<sub>f</sub>: 0.53; <sup>1</sup>H NMR ([D<sub>6</sub>] DMSO):  $\delta$  = 2.09 (s, 2H, CH<sub>2</sub>), 4.67 (s, 1H, CH), 6.18 (s, 2H, benzodioxole C2), 7.14 (d, J = 8, 1H, benzodioxole C6), 7.22 (d, J = 7.5, 1H, benzodioxole C7), 7.25 (t, J = 8, 1H, isatinyl C5), 7.40 (s, 1H, benzodioxole C4), 7.50 (m, J = 6.0, 6.5, 2H, isatinyl C4, C6), 7.67 (d, J = 7.5, 1H, isatinyl C7), 13.60 (s, 1H, NH); <sup>13</sup>C NMR ([D<sub>6</sub>] DMSO):  $\delta$  = 29.16 (propargyl C3), 75.50 (propargyl C1), 77.71 (propargyl C2), 102.73 (benzodioxole C2), 107.86 (benzodioxole C4), 109.11 (benzodioxole C7), 111.05 (isatinyl C7), 119.76 (isatinyl C3a), 121.24 (benzodioxole C5), 123.34 (isatinyl C4), 124.16 (isatinyl C5), 126.34 (isatinyl C6), 132.06 (benzodioxole C6), 136.77 (benzodioxole C3a), 142.18 (benzodioxole C7a), 148.55 (isatinyl C3), 151.752 (isatinyl C7a), 160.75 (isatinyl C=O, C=O); IR (KBr):  $\tilde{\nu}$  = 3244.25 (N-H med), 2980.80 (C-H med), 1436.25 (aromatic C=C str), 1697.35, 1677.29 (C=O str), 1605.51 (C=N med), 1160.91 (C-N str), 1259.00, 1028.27 (C-O str); MS:  $m/z$  = 348 [M+1]; ]; Anal. for C<sub>19</sub>H<sub>13</sub>N<sub>3</sub>O<sub>4</sub>: calc: C (65.70%), H (3.77%), N (12.10%), O (18.43%), found: C (65.72%), H (3.70%), N (12.18%), O (18.40%)

**N'-(3E)-2-oxo-1-(prop-2-en-1-yl)-2,3-dihydro-1H-indol-3-ylidene]-2H-1,3-benzodioxole-5-carbohydrazide (4):** yield: 84.36%; mass: 349.34 gmol<sup>-1</sup>; mp: 192-194 °C; R<sub>f</sub>: 0.56; <sup>1</sup>H NMR ([D<sub>6</sub>] DMSO):  $\delta$  = 4.67 (d, J = 9.5, 2H, CH<sub>2</sub>), 5.00 (m, J = 15.90, 1.56, 9.90, 1.40, 2H, allyl CH<sub>2</sub>), 6.10 (m, J = 15.90, 9.82, 8.45, 1H, allyl CH), 6.18 (s, 2H, benzodioxole C2), 7.20 (d, J = 8.3, 1H, benzodioxole C6), 7.23 (d, J = 8.4, 1H, benzodioxole C7), 7.29 (t, J = 7.5, 1H, isatinyl C5), 7.39 (s, 1H, benzodioxole C4), 7.60 (m, J = 7.5, 8.4, 2H, isatinyl C4, C6), 7.72 (d, J = 8.5, 1H, isatinyl C7), 12.92 (s, 1H, NH); <sup>13</sup>C NMR ([D<sub>6</sub>] DMSO):  $\delta$  = 55.86 (allyl C3), 100.66 (allyl C1), 103.76 (benzodioxole C2), 109.32 (benzodioxole C7, isatinyl C7), 110.18 (allyl C2), 117.32 (benzodioxole C4), 118.63 (isatinyl C3a), 120.45 (isatinyl C5), 121.23 (benzodioxole C5), 122.45 (isatinyl C6), 123.97 (isatinyl C4), 125.67 (benzodioxole C6), 131.23 (isatinyl C7a), 146.78 (benzodioxole C7a, C3a), 149.32 (isatinyl C3), 167.34 (C=O), 168.30 (isatinyl C=O); IR (KBr):  $\tilde{\nu}$  = 2979.34 (C-H med), 1434.33 (aromatic C=C med), 1675 (C=O str), 1610.62 (C=N med), 1164.59 (C-N str), 1097.36,

1028.78 (C-O str), 743.14 (alkene C-H bend str); Anal. for C<sub>16</sub>H<sub>10</sub>N<sub>3</sub>[N<sup>+</sup>]<sub>4</sub>[O<sup>-</sup>]: calc: C (65.32%), H (4.33%), N (12.03%), O (18.32%), found: C (65.28%), H (4.29%), N (12.10%), O (18.33%)

**N'[(3E)-5-nitro-2-oxo-2,3-dihydro-1H-indol-3-ylidene]-2H-1,3-benzodioxole-5-carbohydrazide (5)**: yield: 88.2%; mass: 354.06 gmol<sup>-1</sup>; mp: 295-299 °C; R<sub>f</sub>: 0.78; <sup>1</sup>H NMR ([D<sub>6</sub>] DMSO): δ = 6.17 (s, 2H, benzodioxole C2), 7.09 (d, J = 8, 1H, benzodioxole C6), 7.16 (d, J = 8.4, 1H, benzodioxole C7), 7.30 (s, 1H, benzodioxole C4), 7.36 (d, J = 8.6, 1H, isatiny C7), 7.67 (d, J = 7.5, 1H, isatiny C6), 8.02 (s, 1H, isatiny C4), 10.41 (s, 1H, NH), 12.6 (s, 1H, isatiny NH); <sup>13</sup>C NMR ([D<sub>6</sub>] DMSO): δ = 102.33 (benzodioxole C2), 107.42 (benzodioxole C7), 112.82 (benzodioxole C4), 115.23 (isatiny C4, C7), 119.10 (isatiny C3a), 120.72 (benzodioxole C5), 122.90 (benzodioxole C6), 124.83 (isatiny C5), 135.18 (benzodioxole C3a), 139.17 (benzodioxole C7a), 143.34 (isatiny C7a), 154.87 (isatiny C3), 162.24 (C=O), 163.88 (isatiny C=O); IR (KBr): ν̄ = 3146.13 (N-H str), 1468.80 (aromatic C=C med), 1706.43, 1670.13 (C=O str), 1602.40 (C=N str), 1214.70 (C-N str), 1276.28, 1044.86 (C-O str), 1529.92, 1341.03 (NO<sub>2</sub> str); Anal. for C<sub>19</sub>H<sub>15</sub>N<sub>3</sub>O<sub>4</sub>: calcd: C (54.24%), H (2.85%), N (15.81%), O (27.10%), found: C (54.30%), H (2.76%), N (15.79%), O (27.15%)

**N'[(3E)-5-bromo-2-oxo-2,3-dihydro-1H-indol-3-ylidene]-2H-1,3-benzodioxole-5-carbohydrazide (6)**<sup>34</sup>: yield: 94.6%; mass: 386.99 gmol<sup>-1</sup>; mp: 294-296 °C; R<sub>f</sub>: 0.69; <sup>1</sup>H NMR ([D<sub>6</sub>] DMSO): δ = 6.13 (s, 2H, benzodioxole C2), 6.89 (d, J = 8.3, 1H, benzodioxole C6), 7.13 (d, J = 8.5, 1H, benzodioxole C7), 7.26 (s, 1H, isatiny C4), 7.39 (m, J = 7.5, 8.3, 2H, isatiny C6, C7), 7.62 (s, 1H, benzodioxole C4), 10.7 (s, 1H, NH), 13.2 (s, 1H, isatiny NH); <sup>13</sup>C NMR ([D<sub>6</sub>] DMSO): δ = 102.63 (benzodioxole C2), 104.30 (benzodioxole C4, C7), 112.50 (isatiny C7), 114.34 (isatiny C5), 119.04 (isatiny C3a), 120.45 (benzodioxole C5), 121.36 (isatiny C4), 123.25 (isatiny C6), 125.72 (benzodioxole C6), 136.11 (isatiny C7a), 142.73 (benzodioxole C3a, C7a), 153.45 (isatiny C3), 164.76 (C=O), 164.98 (isatiny C=O); IR (KBr): ν̄ = 3185.7 (N-H med), 2981.09 (C-H med), 1434.41 (aromatic C=C med), 1733.62, 1678.82 (C=O str), 1597.16 (C=N str), 1311.40 (C-N str), 1252.07, 1163.65 (C-O str), 661.73 (C-Br str); Anal. for C<sub>16</sub>H<sub>10</sub>BrN<sub>3</sub>O<sub>4</sub>: calcd: C (49.51%), H (2.60%), Br (20.58%), N (10.83%), O (16.48%), found: C (49.55%), H (2.59%), Br (20.61%), N (10.76%), O (16.49%)

**N'[(3E)-1-benzyl-2-oxo-2,3-dihydro-1H-indol-3-ylidene]-2H-1,3-benzodioxole-5-**

**carbohydrazide (7):** yield: 79.1%; mass: 399 gmol<sup>-1</sup>; mp: 210-213 °C; R<sub>f</sub>: 0.44; <sup>1</sup>H NMR ([D6] DMSO): δ = 5.02 (s, 2H, benzyl CH<sub>2</sub>), 6.18 (s, 2H, benzodioxole C2), 7.07 (d, J = 8.6, 1H, benzodioxole C6), 7.15 (t, J = 7.5, 1H, isatiny C5), 7.19 (m, J = 7.65, 8.24, 8.78, 9.02, 7H, benzyl C2, C3, C4, C5, C6, isatiny C6, benzodioxole C4), 7.50 (d, J = 8.9, 1H, isatiny C7), 7.67 (d, J = 7.4, 1H, benzodioxole C7), 7.79 (d, J = 7.6, 1H, isatiny C4), 13.78 (s, 1H, isatiny NH); <sup>13</sup>C NMR ([D6] DMSO): δ = 50.22 (methylene C), 102.50 (benzodioxole C2), 108.23 (benzodioxole C4), 109.76 (benzodioxole C7), 110.88 (isatiny C7), 114.42 (isatiny C5), 116.12 (isatiny C3a), 119.98 (benzyl C1, C6), 120.54 (benzyl C4), 125.21 (benzodioxole C5, isatiny C6), 128.23 (isatiny C4), 135.76 (benzodioxole C6), 137.55 (benzyl C1), 138.02 (isatiny C7a), 142.21 (benzodioxole C3a), 145.77 (benzodioxole C3a), 153.08 (isatiny C3), 163.88 (C=O), 164.77 (isatiny C=O); IR (KBr): ν̄ = 1437.29 (aromatic C=C med), 1677.49 (C=O str), 1608.71 (C=N str), 1283.93 (C-N str), 1220.20, 1080.70 (C-O str), 1465.40 (methylene C-H med); Anal. for C<sub>23</sub>H<sub>17</sub>N<sub>3</sub>O<sub>4</sub>: calcd: C (69.17%), H (4.29%), N (10.52%), O (16.02%), found C (69.22%), H (4.27%), N (10.52%), O (15.99%)

**N'-(3E)-1-((4-fluorophenyl)methyl)-2-oxo-2,3-dihydro-1H-indol-3-ylidene)-2H-1,3-**

**benzodioxole-5-carbohydrazide (8):** yield: 81.5%; mass: 417.39 gmol<sup>-1</sup>; mp: 199-201 °C; R<sub>f</sub>: 0.52; <sup>1</sup>H NMR ([D6] DMSO): δ = 5.01 (s, 2H, benzyl CH<sub>2</sub>), 6.18 (s, 2H, benzodioxole C2), 7.08 (d, J = 8.6, 1H, benzodioxole C6), 7.15 (t, J = 7.5, 1H, isatiny C5), 7.19 (s, 1H, benzodioxole C4), 7.41 (d, J = 8.4, 1H, benzodioxole C7), 7.47 (m, J = 7.5, 8.3, 8.9, 3H, isatiny C7, benzyl C2, C6), 7.51 (d, J = 8.2, 1H, isatiny C4), 7.53 (d, J = 8.5, 1H, benzyl C5), 7.67 (d, J = 7.5, 1H, benzyl C3), 7.78 (t, J = 7.5, 1H, isatiny C6), 13.76 (s, 1H, NH); <sup>13</sup>C NMR ([D6] DMSO): δ = 42.55 (methylene C), 93.54 (benzodioxole C2), 95.40 (benzodioxole C4), 103.09 (benzodioxole C7), 107.70 (isatiny C7), 109.27 (benzyl C3, C5), 110.84 (benzyl C2), 115.90 (benzyl C6), 116.27 (isatiny C5), 120.15 (isatiny C3a), 121.34 (isatiny C4), 124.26 (benzodioxole C6), 126.34 (benzyl C1), 130.20 (isatiny C7a), 132.23 (benzodioxole C5), 142.96 (isatiny C6), 148.41 (benzodioxole C7a), 150.20 (benzodioxole C3a), 151.83 (isatiny C3), 161.61 (benzyl C4), 202.75 (C=O), 207.30 (isatiny C=O); IR (KBr): ν̄ = 1468 (aromatic C=C med), 1688.40, 1676.85 (C=O str), 1610.80 (C=N str), 1254.54 (C-N str), 1223.64, 1042.30 (C-O str), 1365.25 (C-F str); Anal. for C<sub>23</sub>H<sub>16</sub>FN<sub>3</sub>O<sub>4</sub>: calcd: C (66.18%), H (3.86%), F (4.55%), N (10.07%), O (15.34%), found: C (66.20%), H (3.79%), F (4.58%), N (10.11%), O (15.32%)

**N'-(3E)-5-chloro-1-((4-fluorophenyl)methyl)-2-oxo-2,3-dihydro-1H-indol-3-ylidene)-2H-1,3-benzodioxole-5-carbohydrazide (9):** yield: 92.81%; mass: 451.83 gmol<sup>-1</sup>; mp: 196-199 °C; R<sub>f</sub>: 0.40; <sup>1</sup>H NMR ([D6] DMSO): δ = 5.07 (s, 2H, benzyl CH<sub>2</sub>), 6.17 (s, 2H,

benzodioxole C2), 6.97 (d,  $J = 8.6$ , 1H, benzodioxole C6), 7.13 (t,  $J = 7.8$ , 1H, isatiny C5), 7.21 (d,  $J = 8.4$ , 1H, benzyl C3), 7.30 (m,  $J = 7.4, 8.0, 8.8$ , 3H, isatiny C4, C7, benzyl C2), 7.39 (t,  $J = 7.6$ , 1H, isatiny C6), 7.44 (s, 1H, benzyl C5), 7.48 (d,  $J = 8.6$ , 1H, benzodioxole C7), 7.51 (s, 1H, benzodioxole C4), 13.70 (s, 1H, NH);  $^{13}\text{C}$  NMR ([D6] DMSO):  $\delta = 40.35$  (methylene C), 102.89 (benzodioxole C2), 104.67 (benzodioxole C4), 105.09 (benzodioxole C7), 105.52 (isatiny C7), 117.54 (benzyl C3, C5), 119.14 (benzyl C2), 120.21 (benzyl C6), 123.45 (benzodioxole C5), 129.30 (isatiny C4), 130.45 (isatiny C3a), 134.12 (isatiny C5), 138.05 (benzodioxole C6), 142.76 (benzyl C1), 146.34 (isatiny C7a), 149.18 (isatiny C6), 153.65 (benzodioxole C7a), 154.21 (benzodioxole C3a), 157.67 (isatiny C3), 160.19 (benzyl C4), 167.82 (C=O), 176.75 (isatiny C=O); IR (KBr):  $\tilde{\nu} = 1443.84$  (aromatic C=C med), 1678.83 (C=O str), 1610.10 (C=N med), 1169.59 (C-N med), 1259.45, 1027.10 (C-O str), 746.78 (C-Cl), 1308.61 (C-F med); Anal. for  $\text{C}_{23}\text{H}_{15}\text{ClFN}_3\text{O}_4$ : calcd: C (61.14%), H (3.35%), Cl (7.85%), F (4.20%), N (9.30%), O (14.16%), found: C (61.17%), H (3.33%), Cl (7.80%), F (4.22%), N (9.30%), O (14.18%)

**N'-(3E)-1-((2,4-dichlorophenyl)methyl)-2-oxo-2,3-dihydro-1H-indol-3-ylidene)-2H-1,3-benzodioxole-5-carbohydrazide (10)**: yield: 87.34%; mass: 468.29  $\text{g mol}^{-1}$ ; mp: 220-222 °C; R<sub>f</sub>: 0.42;  $^1\text{H}$  NMR ([D6] DMSO):  $\delta = 5.01$  (s, 2H, benzyl CH<sub>2</sub>), 6.18 (s, 2H, benzodioxole C2), 7.08 (d,  $J = 8.6$ , 1H, benzodioxole C6), 7.15 (t,  $J = 7.5$ , 1H, isatiny C5), 7.19 (s, 1H, benzodioxole C4), 7.41 (d,  $J = 8.4$ , 1H, benzodioxole C7), 7.47 (m,  $J = 7.5, 8.3, 8.9$ , 3H, isatiny C7, benzyl C2, C3), 7.51 (d,  $J = 8.7$ , 1H, isatiny C4), 7.67 (s, 1H, benzyl C5), 7.77 (t,  $J = 7.5$ , 1H, isatiny C6), 13.76 (s, 1H, NH);  $^{13}\text{C}$  NMR ([D6] DMSO):  $\delta = 54.09$  (methylene C), 102.55 (benzodioxole C2), 103.02 (benzodioxole C4), 103.41 (benzodioxole C7), 106.91 (isatiny C7), 110.87 (benzyl C3), 114.31 (benzyl C5), 118.64 (benzyl C2), 119.29 (benzyl C6), 122.18 (benzodioxole C5), 126.14 (isatiny C4), 127.51 (isatiny C3a), 132.81 (isatiny C5), 136.33 (benzyl C4), 141.75 (benzodioxole C6), 144.91 (benzyl C1), 147.89 (isatiny C7a), 150.11 (isatiny C6), 152.44 (benzodioxole C7a), 157.23 (benzodioxole C3a), 158.36 (isatiny C3), 166.17 (C=O), 179.91 (isatiny C=O); IR (KBr):  $\tilde{\nu} = 1438.79$  (aromatic C=C med), 1679.78 (C=O str), 1609.53 (C=N med), 1171.38 (C-N str), 1254.46, 1025.02 (C-O str), 751.30, 685.34 (C-Cl str); Anal. for  $\text{C}_{23}\text{H}_{15}\text{Cl}_2\text{N}_3\text{O}_4$ : calcd: C (58.99%), H (3.23%), Cl (15.14%), N (8.97%), O (13.67%), found: C (58.97%), H (3.29%), Cl (15.13%), N (8.99%), O (13.62%)

### ***In vitro* MAO inhibition studies**

Rat brain mitochondrial extract was procured from The Neuropharmacology Lab, Department of Pharmaceutical Engineering and Technology, IIT (BHU) for carrying out the *in vitro* MAO enzyme inhibition assay. The selected compounds **2-4**, **7**, **8**, and **10** were used for the MAO inhibition assay according to a previously reported procedure by Tabor et al. The protein content in the rat mitochondria extract was estimated using the technique described by Lowry et al. using bovine albumin as the standard. All the compounds tested were dissolved in DMSO, and the buffer solution was added in such a manner that the final DMSO concentration was measured at 4%, off limits of possible inhibition with the proteins under inspection. The standard drugs selegiline and clorgiline were used as reference standards for MAO-B and MAO-A assay respectively. The IC<sub>50</sub> values were calculated at 95% confidence limits using GraphPad Prism 5.0 from the plots of inhibition percentages vs logarithm of inhibition concentration.

### MAO inhibition assay

The fresh rat brain mitochondrial suspension was prepared and procured from the Neuropharmacology lab, Department of Pharmaceutical Engineering and Technology, which was estimated and further prepared to give a working solution of 0.84 (mg protein) mL<sup>-1</sup>. A volume of 55 μL of the mitochondrial suspension was added with 90 μL of 50 mM Tris-HCl buffer (pH: 8.2), and 30 mL of solubilizing solution, which can be the control or inhibitor solution of five distinct concentrations, to eventually prepare an aliquot. The enzyme reaction was activated by the addition of 25 μL of 5-HT (4 mM, substrate for MAO-A) evaluating MAO-A response or 25 μL of benzylamine (0.1 M, MAO-B substrate) for determining MAO-B activity. The mixture was then incubated at 37°C, human body temperature, for 30 min, after which the reaction was terminated by adding 50 μL of 1 N HCl. The absorbance for the supernatants, thus obtained, was measured at a wavelength of 280 nm as in the case of MAO-A (formation of 5-hydroxyindoleacetic acid) and at 250 nm for MAO-B estimation (formation of benzaldehyde)<sup>[25]</sup>. All the assays were performed in triplicate and were repeated twice. Control and blank tests were also performed, without inhibitor and protein suspension respectively.

### Reversibility and irreversibility of MAO-B inhibition

To investigate whether the observed enzyme inhibition was reversible or irreversible, time-dependent inhibition studies were carried with the lead inhibitors **2** and **3** with rMAO-B using a method described by Legoabe et al. with slight modifications. Compounds **2** and **3** were pre-incubated with the mitochondrial working solution (0.78 [mg protein] mL<sup>-1</sup>) for various periods of time (0, 15, 30, 60

min) at 37°C in Tris·HCl buffer (50 mM, pH 8.2). For this purpose, the concentration of both the compounds was equal to two-fold the measured IC<sub>50</sub> value for the inhibition of MAO-B (118 nM). The reactions were subsequently diluted two-fold by the addition of 0.1M benzylamine to yield a final enzyme concentration of 0.39 mgmL<sup>-1</sup> and inhibitor concentration that was equal to the IC<sub>50</sub> value. The reaction was incubated at 37°C for a further 15 min, and the residual enzyme activity was measured and bar graphs were constructed. All measurements were carried out in triplicate and are expressed as the mean ± standard error of the mean (SEM).

### ***In vitro* ChE inhibitory activity**

All the compounds were tested to determine the *in vitro* potency against the ChE enzymes. For the study eeAChE and eqBChE were used. Acetylthiocholine iodide (ACTI) was used as the substrate for the AChE inhibition assay, which follows a modified colorimetric method described by Ellman et al., using 5,5'-Dithiobis(2-nitro-benzoic acid) (DTNB). About 30 µL of the enzyme (AChE) was added to 60 µL of sodium phosphate buffer (20 mM, pH 7.4), and kept for incubation after adding 30 µL of DTNB (10 mM) solution with different inhibitor concentrations. The system was incubated at 25°C for 15 min. The absorbance was measured at 415 nm (formation of hydrolysis products) with the help of 96-well microplate reader<sup>[26]</sup>. The control experiments involved the exclusion of inhibitors in the assay, while the blanks were calculated without the enzyme. All assays were performed in the triplicate measure. For the inhibition studies for BChE enzyme, the protocol adapted was the same developed for AChE, with the exception of the enzyme and the substrate, where eqBChE and butyrylthiocholine iodide (BuTi) was used respectively<sup>[20]</sup>. The IC<sub>50</sub> values were calculated at 95% confidence limits with the help of GraphPad Prism 5.0 from the percentage inhibition vs logarithm inhibition concentration plot.

### **Reversibility and irreversibility of AChE inhibition**

To investigate whether the observed enzyme inhibition was reversible or irreversible, time-dependent inhibition studies were carried with the representative inhibitors, compounds **2** and **3**. The selected leads were pre-incubated with the AChE enzyme for various time periods (0, 15, 30, 60 min) at 25°C in sodium phosphate buffer (20 mM, pH 7.4) and DTNB solution (10 mM). For this purpose, the chosen concentration of the inhibitors was equal to two-fold the measured IC<sub>50</sub> value for the inhibition of AChE (17.4 nM). The reaction was subsequently diluted two-fold by the addition of ACTI (0.8 mM), such that the inhibitor concentration was equal to the IC<sub>50</sub> value. The reaction was incubated at

258Cf or a further 15 min, and the residual enzyme activities were measured, and bar graphs were constructed. All measurements were carried out in triplicate and are expressed as mean  $\pm$  SEM.

### **Molecular docking studies**

For the molecular modeling (MM) studies, all the important software packages were installed and operated on HP Z230 Desktop Workstation based on Windows 7 (x86) OS. The packages used for the study include ChemDraw 12.0 Pro and Chem3D Ultra for drawing and optimising chemical structures respectively, Molecular Graphics Laboratory (MGL) tools 1.5.4, AutoDock 4.2 (docking studies), Discovery Studio 2017 R<sub>2</sub> Client (protein-ligand interaction visualization and editing), and Pymol visualizer 2.2.3 (GSP determination and protein visualisation). For the protein-ligand studies, the required PDB structures were selected after a thorough process of screening based on the requirement of enzyme conformation and other parameters from all the deposited structures in RCSB PDB. For the enzymes of the present study AChE, BChE, MAO-A and MAO-B, the co-crystallized structures with PDB ID: 4EY7, 5DYW, 2Z5X, and 2V5Z were chosen respectively<sup>[27]</sup>. For the protein-ligand interaction studies, via molecular docking, only one subunit of the participating enzymes were used, i.e., the  $\beta$ -chain was removed in all the cases along with the bound inhibitors. The water molecules associated with the structures, along with other solvents or ions were removed using Discovery Studio 2017 R<sub>2</sub> Client visualizer software. The refined structures were prepared further using AutoDock Tools (ADT), where missing hydrogen atoms and bond orders were assigned, followed calculation of Gasteiger-Marsili and Kollman charges. The resultant structure was further edited by merging the non-polar hydrogens, after which it was saved into .pdbqt file type. The structure of the compounds under investigation, as well as the inhibitors present in the co-crystallized protein complex, was drawn using ChemDraw 12.0 Pro and optimized using Chem3D Ultra and saved in .pdb format. These structures were then loaded into ADT and were saved in .pdbqt format after assigning rotatable bonds<sup>[28]</sup>. The molecular docking studies were performed using a previously developed protocol for all the enzymes.

### ***In silico* drug-likeness and pharmacokinetic parameter prediction studies**

All the designed compounds were subjected to proper filters to determine the potential to be developed as drugs. To address the drug-like properties, all the molecules were screened using the online PreADMET server<sup>[35]</sup>, where the Lipinski rule of five principles was applied. This screening parameter is crucial in determining preliminary leads with better solubility and permeability profile.

All the compounds satisfied the Lipinski filter, which defines optimal conditions for the properties hydrogen bond donor ( $\leq 5$ ) and acceptor ( $\leq 10$ ), molecular weight ( $\leq 500$ ), and partition coefficient, Clog P, ( $\leq 5$ ), and in the appropriate range for greater probability of translation into clinical candidates. This further strengthened the possibility of the compounds to be developed further into potent MTDLs. The results are presented in **Table 4**.

## Acknowledgments

The authors thank the Design and Innovation Center (DIC), IIT (BHU), for financial support. Also acknowledge Dr. Sushil Kumar Singh and Dr. Sairam Krishnamurthy, Department of Pharmaceutical Engineering and Technology, Indian Institute of Technology (Banaras Hindu University), Varanasi for their key role in assisting the pharmacological screening.

**Keywords:** Piperonylic acid. hydrazones. monoamine oxidase inhibitors. acetylcholinesterase. molecular docking

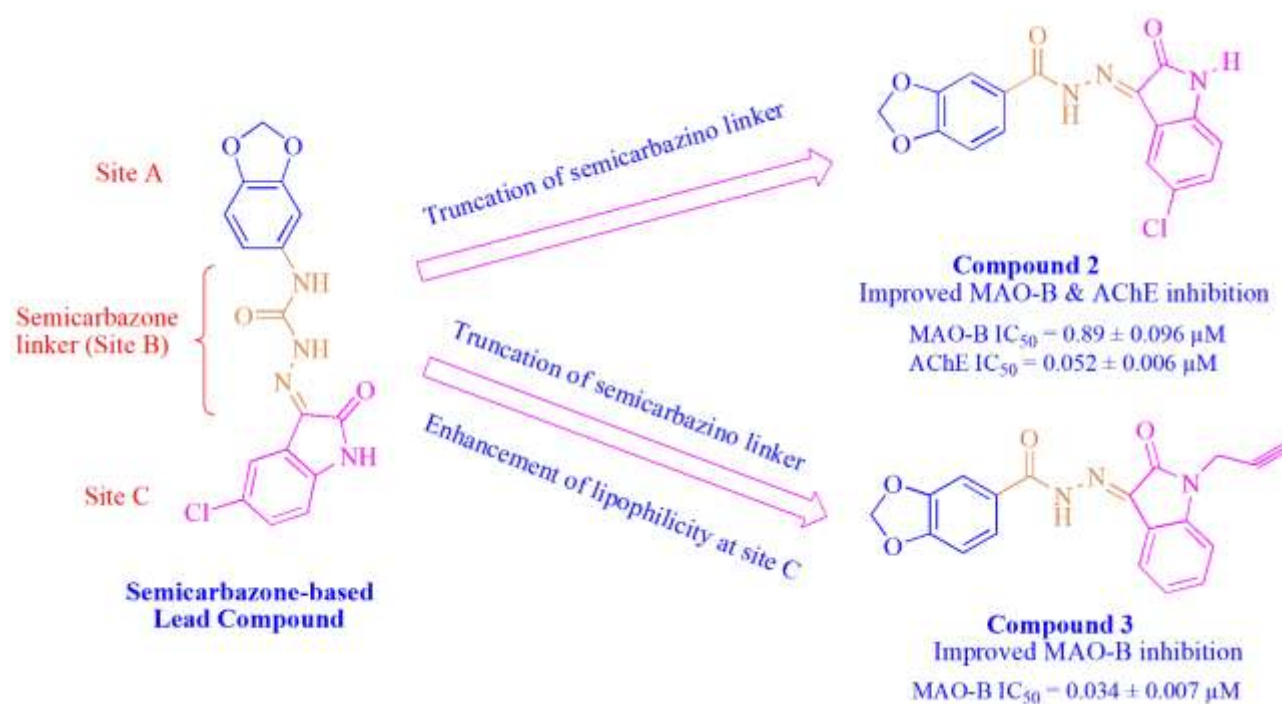
## References

- [1] L. De Colibus, M. Li, C. Binda, A. Lustig, D. E. Edmondson, A. Mattevi, *Proc. Natl. Acad. Sci.* **2005**, *102*, 12684–12689.
- [2] D. E. Edmondson, P. Newton-Vinson, *Antioxid. Redox Signal.* **2001**, *3*, 789–806.
- [3] H. Dvir, I. Silman, M. Harel, T. L. Rosenberry, J. L. Sussman, *Chem. Biol. Interact.* **2010**, *187*, 10–22.
- [4] M. B. H. Youdim, D. Edmondson, K. F. Tipton, *Nat. Rev. Neurosci.* **2006**, *7*, 295–309.
- [5] L. Fang, Y. Pan, J. L. Muzyka, C.-G. Zhan, *J. Phys. Chem. B* **2011**, *115*, 8797–8805.
- [6] A. Nordberg, C. Ballard, R. Bullock, T. Darreh-Shori, M. Somogyi, *Prim. Care Companion CNS Disord.* **2013**, *15*, DOI 10.4088/PCC.12r01412.
- [7] S. N. Dighe, G. S. Deora, E. De la Mora, F. Nachon, S. Chan, M.-O. Parat, X. Brazzolotto, B. P. Ross, *J. Med. Chem.* **2016**, *59*, 7683–7689.
- [8] C. A. Taylor, S. F. Greenlund, L. C. McGuire, H. Lu, J. B. Croft, *MMWR Morb. Mortal. Wkly. Rep.* **2017**, *66*, 521–526.
- [9] P. V. Fish, D. Steadman, E. D. Bayle, P. Whiting, *Bioorg. Med. Chem. Lett.* **2019**, *29*, 125–133.

- [10] A. Haapasalo, M. Hiltunen, *Neurodegener. Dis. Manag.* **2018**, *8*, 289–299.
- [11] S. L. Greig, *CNS Drugs* **2015**, *29*, 963–970.
- [12] S. O. Bachurin, E. V. Bovina, A. A. Ustyugov, *Med. Res. Rev.* **2017**, *37*, 1186–1225.
- [13] M. B. H. Youdim, Y. S. Bakhle, *Br. J. Pharmacol.* **2009**, *147*, S287–S296.
- [14] A. Cavalli, M. L. Bolognesi, A. Minarini, M. Rosini, V. Tumiatti, M. Recanatini, C. Melchiorre, *J. Med. Chem.* **2008**, *51*, 347–372.
- [15] P. W. Rose, C. Bi, W. F. Bluhm, C. H. Christie, D. Dimitropoulos, S. Dutta, R. K. Green, D. S. Goodsell, A. Prlić, M. Quesada, G.B. Quinn, A.G. Ramos, J.D. Westbrook, J. Young, C. Zardecki, H.M. Berman, P.E. Bourne, *Nucleic Acids Res.* **2012**, *41*, D475–D482.
- [16] J. Marco-Contelles, M. Unzeta, I. Bolea, G. Esteban, R. R. Ramsay, A. Romero, R. Martínez-Murillo, M. C. Carreiras, L. Ismaili, *Front. Neurosci.* **2016**, *10*, DOI 10.3389/fnins.2016.00294.
- [17] J. Joubert, G. B. Foka, B. P. Repsold, D. W. Oliver, E. Kapp, S. F. Malan, *Eur. J. Med. Chem.* **2017**, *125*, 853–864.
- [18] S.-S. Xie, X. Wang, N. Jiang, W. Yu, K. D. G. Wang, J.-S. Lan, Z.-R. Li, L.-Y. Kong, *Eur. J. Med. Chem.* **2015**, *95*, 153–165.
- [19] J. Marco-Contelles, O. Bautista-Aguilera, G. Esteban, M. Chioua, K. Nikolic, D. Agbaba, I. Moraleda, I. Iriepa, E. Soriano, A. Samadi, M. unzeta, J. Marco-Contelles, *Drug Des. Devel. Ther.* **2014**, 1893-1910.
- [20] R. K. P. Tripathi, V. M. Sasi, S. K. Gupta, S. Krishnamurthy, S. R. Ayyannan, *J. Enzyme Inhib. Med. Chem.* **2018**, *33*, 37–57.
- [21] A. Medvedev, O. Buneeva, V. Glover, *Biol. Targets Ther.* **2007**, *1*, 151–162.
- [22] A. Ogata, N. Hamaue, M. Terado, M. Minami, K. Nagashima, K. Tashiro, *J. Neurol. Sci.* **2003**, *206*, 79–83.
- [23] C. I. Manley-King, J. J. Bergh, J. P. Petzer, *Bioorg. Med. Chem.* **2011**, *19*, 261–274.
- [24] B. R. Boar, D. M. O'shea, I. D. Tomlinson, *1-Substituted Isatin and Oxindole Derivatives as Inhibitors of Acetylcholinesterase*, **1994**, WO1994029272A1.
- [25] R. K. P. Tripathi, G. K. Rai, S. R. Ayyannan, *ChemMedChem* **2016**, *11*, 1145–1160.
- [26] R. K. P. Tripathi, S. R. Ayyannan, *Med. Chem. Res.* **2018**, *27*, 709–725.
- [27] G. L. Warren, T. D. Do, B. P. Kelley, A. Nicholls, S. D. Warren, *Drug Discov. Today* **2012**, *17*, 1270–1281.
- [28] D. Seeliger, B. L. de Groot, *J. Comput. Aided Mol. Des.* **2010**, *24*, 417–422.
- [29] D. E. V. Pires, T. L. Blundell, D. B. Ascher, *J. Med. Chem.* **2015**, *58*, 4066–4072.
- [30] M. N. Drwal, P. Banerjee, M. Dunkel, M. R. Wettig, R. Preissner, *Nucleic Acids Res.* **2014**, *42*, W53–W58.

- [31] S. D. Joshi, H. M. Vagdevi, V. P. Vaidya, G. S. Gadaginamath, *Eur. J. Med. Chem.* **2008**, *43*, 1989–1996.
- [32] B. Strydom, S. F. Malan, N. Castagnoli, J. J. Bergh, J. P. Petzer, *Bioorg. Med. Chem.* **2010**, *18*, 1018–1028.
- [33] L. J. Legoabe, A. Petzer, J. P. Petzer, *Eur. J. Med. Chem.* **2012**, *49*, 343–353.
- [34] Y. Zhong, M. Xue, X. Zhao, J. Yuan, X. Liu, J. Huang, Z. Zhao, H. Li, Y. Xu, *Bioorg. Med. Chem.* **2013**, *21*, 1724–1734.
- [35] L. Zhou, Y. Zhu, Y. Jiang, X. Zhao, D. Guo, *Bioorg. Med. Chem. Lett.* **2017**, *27*, 4180–4184.

### Graphical Abstract



A set of piperonylic acid derived hydrazones with variable isatin moiety was synthesized and evaluated for their inhibitory activity against the enzymes acetylcholinesterase (AChE), butyrylcholinesterase (BChE), and monoamine oxidase A and B (MAO-A/B). The compound **3** was identified as lead AChE inhibitor with  $IC_{50} = 0.052 \pm 0.006 \mu\text{M}$  while compound **2** proved to be a lead MAO-B inhibitor with  $IC_{50} = 0.034 \pm 0.007 \mu\text{M}$ , possessing 50 times more selectivity than MAO-A. The kinetic studies revealed that compounds **2** and **3** displayed competitive and reversible inhibition of AChE ( $K_i = 6.22 \pm 0.002 \text{ nM}$ ) and MAO-B ( $K_i = 12.14 \pm 0.026 \text{ nM}$ ) respectively. The molecular docking studies revealed the significance of hydrophobic interactions along the active site pocket of the enzymes under

inspection. *In-silico* molecular and ADME properties further supported the drug-like characteristics of these compounds.

Accepted Manuscript